# WiBorder: Precise Wi-Fi based Boundary Sensing via Through-wall Discrimination

Shengjie Li, Zhaopeng Liu, Yue Zhang, Qin Lv, Xiaopeng Niu, Leye Wang, Daqing Zhang

# WiBorder: Precise Wi-Fi based Boundary Sensing via Through-wall Discrimination

SHENGJIE LI, ZHAOPENG LIU, and YUE ZHANG, Peking University, China
QIN LV, University of Colorado Boulder, USA
XIAOPENG NIU and LEYE WANG, Peking University, China
DAQING ZHANG*, Peking University, China and Telecom SudParis, France

Recent research has shown great potential of exploiting Channel State Information (CSI) retrieved from commodity Wi-Fi devices for contactless human sensing in smart homes. Despite much work on Wi-Fi based indoor localization and motion/intrusion detection, no prior solution is capable of detecting a person entering a room with a precise sensing boundary, making room-based services infeasible in the real world. In this paper, we present WiBorder, an innovative technique for accurate determination of Wi-Fi sensing boundary. The key idea is to harness antenna diversity to effectively eliminate random phase shifts while amplifying through-wall amplitude attenuation. By designing a novel sensing metric and correlating it with human's through-wall discrimination, WiBorder is able to precisely determine Wi-Fi sensing boundaries by leveraging walls in our daily environments. To demonstrate the effectiveness of WiBorder, we have developed an intrusion detection system and an area detection system. Extensive results in real-life scenarios show that our intrusion detection system achieves a high detection rate of 99.4% and a low false alarm rate of 0.68%, and the area detection system's accuracy can be as high as 97.03%. To the best of our knowledge, WiBorder is the first work that enables precise sensing boundary determination via through-wall discrimination, which can immediately benefit other Wi-Fi based applications.

CCS Concepts: • **Human-centered computing → Ubiquitous and mobile computing systems and tools**.

Additional Key Words and Phrases: Wi-Fi; Channel State Information (CSI); Device-free Sensing; Sensing boundary; Intrusion Detection; Area Detection

**ACM Reference Format:**
Shengjie Li, Zhaopeng Liu, Yue Zhang, Qin Lv, Xiaopeng Niu, Leye Wang, and Daqing Zhang. 2020. WiBorder: Precise Wi-Fi based Boundary Sensing via Through-wall Discrimination. *Proc. ACM Interact. Mob. Wearable Ubiquitous Technol.* 4, 3, Article 89 (September 2020), 30 pages. https://doi.org/10.1145/3411834

*This is the corresponding author.

Authors' addresses: Shengjie Li, lishengjie@pku.edu.cn; Zhaopeng Liu, liuzp@pku.edu.cn; Yue Zhang, zy.zhang@pku.edu.cn, Peking University, Key Laboratory of High Confidence Software Technologies (Ministry of Education), School of Electronics Engineering and Computer Science, Peking University, Beijing, China; Qin Lv, qin.lv@colorado.edu, University of Colorado Boulder, Department of Computer Science, University of Colorado Boulder, Boulder, USA; Xiaopeng Niu, nxpeng@pku.edu.cn; Leye Wang, leyewang@pku.edu.cn, Peking University, Key Laboratory of High Confidence Software Technologies (Ministry of Education), School of Electronics Engineering and Computer Science, Peking University, Beijing, China; Daqing Zhang, dqzhang@sei.pku.edu.cn, Peking University, Key Laboratory of High Confidence Software Technologies (Ministry of Education), School of Electronics Engineering and Computer Science, Peking University, Beijing, China, Telecom SudParis, Institut Mines, Telecom SudParis, Evry, France, Evry, France.


2474-9567/2020/9-ART89 $15.00
https://doi.org/10.1145/3411834

## 1 INTRODUCTION

In recent years, with the rapid development of wireless technologies, the role of Wi-Fi Radio Frequency (RF) signal has been extended from a sole communication medium to a non-intrusive environmental sensing tool. Compared with other contactless (a.k.a, device-free) sensing techniques such as camera-based [32, 34] or ultrasound-based [8, 44, 55] approaches, one key advantage of Wi-Fi sensing is its ubiquity in indoor environments, requiring no extra infrastructure deployment. By 2019, more than 13 billion active Wi-Fi devices have been deployed around the globe [47].

In a typical indoor environment, Wi-Fi signals propagate not only along the Line-of-Sight (LoS) path from the transmitter to the receiver, but also through multi-paths, reflected by one or more objects before arriving at the receiver, hence carrying information about the environment. By analyzing the received RF signal patterns and characteristics, many Wi-Fi based human sensing applications have been developed, ranging from coarse-grained sensing such as activity recognition [7, 15, 40, 43, 45], indoor localization/tracking [21, 25, 26, 35, 42, 54, 56], and motion detection [20, 24, 27, 36, 50, 53, 59], to fine-grained sensing like respiration monitoring [28, 58, 60]. A lot of these applications require prior knowledge of whether a target has entered the sensing area of interest. For example, intrusion detection applications need to know whether someone has entered a house in order to raise an intrusion alarm in time. It is particularly important for such applications to accurately detect a person entering the house (i.e., crossing a precise boundary) and avoid false alarms caused by human motion outside the house. As another example, smart home applications need to know which area the sensing target is in, so as to provide location-aware services, e.g., turning on light when a user enters the bathroom. Moreover, it is well known that activities are closely related to areas, e.g., sleeping in the bedroom and cooking in the kitchen. As such, knowing the area provides important location-related context for activity recognition systems. Given that a target is in a specific area (e.g., bathroom) and fewer activities can be conducted in that area, the number of candidate activities to consider is much smaller in the classification process, which can significantly reduce the complexity of activity recognition.

Ideally, we would like to draw a clear line (i.e., precise boundary sensing) to determine whether a human target has entered a sensing area or not. Although much research has been conducted to detect human motion state or locate human target, several limitations still remain when applying these methods to determine clear sensing boundaries in real-life scenarios. On the one hand, existing approaches usually detect human motion by extracting time-domain or frequency-domain features from Wi-Fi signals, such as variance or correlation from the time domain and Doppler frequency shift from the frequency domain. These methods are proposed to detect human motion within the sensing range of Wi-Fi devices. However, the coverage of Wi-Fi signals is quite large (e.g., 46m for 2.4GHz [48]), and so is the sensing range of those systems, resulting in a fuzzy sensing boundary. Conversely, Wi-Fi based human sensing usually requires accurate detection of a human target's presence within a given area of interest. Such requirements call for a method to determine a clear sensing boundary for the given area. On the other hand, previous works have also attempted to localize human target using fingerprinting-based methods or geometric mapping-based methods. To the best of our knowledge, the 90th percentile error of current device-free localization methods can be as large as 2m [12]. Such localization accuracy is insufficient for determining precise sensing boundary in real-life scenarios.

In this paper, to address the limitations mentioned above, we present WiBorder, a novel solution that takes advantage of common walls that exist in indoor environments for precise sensing boundary determination. By utilizing the wall and wall's extension, we'd like to obtain a clear line (i.e., boundary) to determine whether a human target has crossed the line or not. By observing the human reflected signal strength distribution inside or outside a wall, we find that the distribution changes gradually inside the wall when there is a direct reflected path off the human body, but drops significantly when the person moves from inside to outside and the direct reflected path becomes indirect (i.e., through-wall). By measuring the distribution continuously in

real-time, we can determine whether a person is inside or outside a precise boundary via through-wall signal discrimination. Specifically, we employ two antennas on the receiver, which are widely available on commodity Wi-Fi devices for performance boosting. We first apply CSI conjugate multiplication between the two antennas, which not only eliminates the time-varying phase shift in raw CSI, but also amplifies through-wall amplitude attenuation. Then from the conjugate-multiplying CSI, we construct an effective CSI metric called DCM-CSI to characterize the human reflected signal strength distribution, which has the strong capability of precise boundary sensing via through-wall signal discrimination. Furthermore, through a detailed investigation that establishes the corresponding relationship between DCM-CSI and human movement, we explain this boundary sensing capability theoretically and validate it through extensive empirical studies. Finally, to evaluate the effectiveness of WiBorder, we have conducted extensive real-world experiments with two case studies: an intrusion detection system and an area detection system. A demo video is also submitted as attached material to demonstrate the effectiveness of our proposed techniques in these two case studies.

The main contributions of this work can be summarized as follows:

(1) For the first time, we propose a precise sensing boundary determination method called WiBorder, taking advantage of common walls in our daily life. To achieve this, we design an effective metric (DCM-CSI) which is extracted from CSI conjugate multiplication between two antennas and is effective for discrimination of inside-wall and outside-wall activities.
(2) We develop the mathematical relationship between human movement and DCM-CSI, and theoretically explain DCM-CSI's capability for precise boundary sensing. Moreover, we have conducted extensive empirical studies to validate this capability.
(3) We have conducted two case studies in real-life scenarios to fully demonstrate the effectiveness of WiBorder. The first is an intrusion detection system, which achieves a high detection rate of 99.4% and a low false alarm rate of 0.68%. The second is an area detection system that achieves a high area detection accuracy of 97.03%. Furthermore, we have conducted an in-situ experiment to test the feasibility of our area detection system for multi-area trajectory recording, and the result demonstrates its potential for behavioral analysis of multi-person movements in indoor environments.

The rest of this paper is organized as follows. Sec. 2 presents DCM-CSI, the new CSI metric and its relationship with human movement. Sec. 3 presents extensive empirical studies to demonstrate the unique property of DCM-CSI for Wi-Fi sensing boundary determination. Sec. 4 describes two case studies to fully evaluate the effectiveness of WiBorder. Sec. 5 surveys related work. Sec. 6 offers some guidance for device deployment and discusses more opportunities for WiBorder. Finally, Sec. 7 concludes this work.

## 2 DCM-CSI: A NEW CSI METRIC FOR THROUGH-WALL DISCRIMINATION

In this section, we first present the intuition of WiBorder and introduce how we realize this intuition by extracting an effective metric from Wi-Fi CSI. In order to derive this new metric, we first lay the foundation by introducing the basic concept of CSI, then detail the effect of human movement on CSI and conjugate-multiplying CSI of two antennas. Finally, we describe how to derive DCM-CSI, the new CSI metric from conjugate-multiplying CSI, and reveal the theoretical relationship between human movement and DCM-CSI.

### 2.1 Intuition of WiBorder

The inspiration of WiBorder comes from the observation that, in typical indoor environments, sensing areas of interest are usually at room level, with distinctive characteristics of being divided by walls. These walls naturally form the boundaries between different spaces and play an important role in real-world sensing applications. Take intrusion detection as an example, the sensing boundaries are walls of a target house. As for area detection in a smart home, the sensing area is typically a room of interest (e.g., bathroom or bedroom), which is usually defined

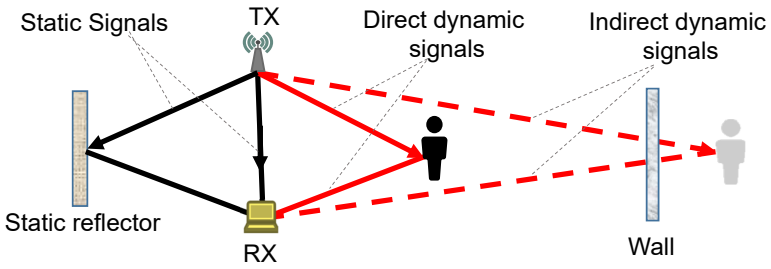


Fig. 1. Illustration of Wi-Fi multi-path propagation in an indoor environment, and the difference between direct dynamic signal and indirect (i.e., through-wall) dynamic signal.

by walls around it. Therefore, if we could capture certain features from Wi-Fi signals to discriminate between inside-wall and outside-wall activities, then it would be easy to determine precise sensing boundaries using walls in the environment.

Before answering the question of how to discriminate between inside-wall and outside-wall activities, we first introduce two basic concepts: direct dynamic signal and indirect dynamic signal. As shown in Figure 1, among all the multi-path propagation signals within an environment, there are static signals (signals that are reflected by static objects such as walls or furniture), and dynamic signals (signals that are reflected by moving human target). Dynamic signals can further be divided into two types: (1) direct dynamic signals (abbreviated as **direct signals**): signals that are directly reflected by a moving human target when propagating from the transmitter to the receiver; (2) indirect dynamic signals (abbreviated as **indirect signals**): signals that are reflected by a moving human target but penetrate through walls along their propagation. Once the transceivers are deployed, inside-wall and outside-wall activities will cause different types of dynamic signals. As such, if we can differentiate between direct and indirect signals, we are able to discriminate inside-wall and outside-wall activities. To achieve this, WiBorder first applies conjugate multiplication between Wi-Fi CSI readings of the receiver's two antennas, which not only eliminates time-varying phase shift in the raw CSI, but also amplifies through-wall amplitude attenuation [26]. Then we construct DCM-CSI, a novel CSI metric from the conjugate-multiplying CSI, capable of distinguishing direct and indirect signals.

In the following sections, we will introduce the effect of human movement on CSI and the two-antenna conjugate-multiplying CSI, and present the derivation of DCM-CSI in details.

## 2.2 Primer of CSI and CSI Conjugate Multiplication

Due to multi-path propagation in a typical indoor environment, the Wi-Fi signal received at the receiver is a superposition of signals from all paths. As a consequence, the CSI can be expressed as:

$$H(f, t_0 + t) = \sum_{l=1}^{L} \alpha_l(t_0 + t) e^{-j2\pi f \tau_l(t_0+t)}, \tag{1}$$

where $L$ is the number of propagation signals, $\tau_l(t_0 + t)$ is the propagation delay of the $l$-th signal at time $t_0 + t$, and $\alpha_l(t_0 + t)$ is the amplitude attenuation. These propagation signals can be further grouped into static signals and dynamic signal, where the static signals do not change with time, and the dynamic signals change with the movement of human targets [43]. Then, the CSI can be rewritten as:

$$H(f, t_0 + t) = \sum_{s=1}^{S} \alpha_s e^{-j2\pi f \tau_s} + \sum_{d=1}^{D} \alpha_d(t_0 + t) e^{-j2\pi f \tau_d(t_0+t)}, \tag{2}$$

where $S$ is the set of static signals, and $D$ is the set of dynamic signals. After merging static part of signals into a constant complex value, we simplify the CSI expression as:

$$H(f, t_0 + t) = A_s e^{j\phi_s} + \sum_{d=1}^{D} \alpha_d(t_0 + t) e^{j\phi_d(t_0+t)}, \tag{3}$$

where $A_s e^{j\phi_s}$ is the CSI of merged static signals and $\alpha_d(t_0 + t), \phi_d(t_0 + t)$ are the amplitude attenuation and phase change of the $d$-th dynamic signal, respectively. As the human target moves in the environment, the path length of dynamic signals changes accordingly, resulting in changes of $\alpha_d(t_0 + t), \phi_d(t_0 + t)$. In other words, the change of CSI can be utilized to characterize the human target movement. However, since the receivers are not strictly synchronized in carrier frequency with the transmitters on commodity devices, there is a time-varying random phase offset $e^{\theta_{offset}}$ in each CSI sample, shown as follows:

$$H(f, t_0 + t) = e^{j\theta_{offset}}(A_s e^{j\phi_s} + \sum_{d=1}^{D} \alpha_d(t_0 + t) e^{j\phi_d(t_0+t)}) \tag{4}$$

This random phase offset can have a significant impact on CSI, thus interferes with the mapping between CSI change and human movement. To eliminate this random phase offset, we can apply conjugate multiplication between the CSI readings from two antennas. This works because different antennas on the same Wi-Fi card (e.g., Intel 5300 Wi-Fi card has three antennas) share the same RF oscillator, so the time-varying random phase offsets are the same across different antennas [26].

After conjugate multiplication, as expressed in Equation 5, conjugate-multiplying CSI is composed of four components. The first component is the product of static CSI of the first antenna and conjugate-static CSI of the second antenna. The second component is the product of static CSI of the first antenna and conjugate-dynamic CSI of the second antenna. The third component is the product of dynamic CSI of the first antenna and conjugate-static CSI of the second antenna. And the fourth component is the product of dynamic CSI of the first antenna and conjugate-dynamic CSI of the second antenna.

$$\begin{aligned} H_1(f, t_0 + t) \cdot H_2^*(f, t_0 + t) &= (A_{s_1} e^{j\phi_{s_1}} + \sum_{d1=1}^{D1} \alpha_{d1}(t_0 + t) e^{j\phi_{d1}(t_0+t)}) \cdot (A_{s_2} e^{-j\phi_{s_2}} + \sum_{d2=1}^{D2} \alpha_{d2}(t_0 + t) e^{-j\phi_{d2}(t_0+t)}) \\ &= \underbrace{A_{s_1} A s_2 e^{j(\phi_{s_1} - \phi_{s_2})}}_{1} + \underbrace{A_{s_1} \sum_{d2=1}^{D2} \alpha_{d2}(t_0 + t) e^{-j(\phi_{d2}(t_0+t) + \phi_{s_1})}}_{2} + \underbrace{A_{s_2} \sum_{d1=1}^{D1} \alpha_{d1}(t_0 + t) e^{j(\phi_{d1}(t_0+t) - \phi_{s_2})}}_{3} \\ &\quad + \underbrace{\sum_{d1=1}^{D1} \alpha_{d1}(t_0 + t) e^{j\phi_{d1}(t_0+t)} \sum_{d2=1}^{D2} \alpha_{d2}(t_0 + t) e^{-j\phi_{d2}(t_0+t)}}_{4} \end{aligned} \tag{5}$$

## 2.3 From CSI Conjugate Multiplication to DCM-CSI

As shown above, after conjugate multiplication, the expression is quite complex. To further simplify the above expression, we have three key observations:

- For two close-by antennas on the same Wi-Fi card, they share the same number of incoming signals, which means $D1 = D2$ [25, 58]. Moreover, the amplitude attenuation of a dynamic signal reaching two close-by antennas can be considered as similar [25]. Therefore, $\alpha_{d1}(t_0 + t)$ and $\alpha_{d2}(t_0 + t)$ can be expressed as $\alpha_d(t_0 + t)$.
- When human moves for a short distance, the change of the amplitude $\alpha_d(t_0 + t)$ is very small, which can be regarded as a constant $\alpha_d(t_0)$ in a short time window [33].

- Compared with the amplitude of merged static signals($A_{s_1}$ or $A_{s_2}$), the amplitude $\alpha_d(t_0+t)$ of dynamic signals is very small, thus the fourth component of conjugate-multiplying CSI is small enough to be ignored [26].

Based on these observations, we can simplify CSI conjugate multiplication as shown in Equation 6, in which $\phi_d^1(t_0+t)$, $\phi_d^2(t_0+t)$ represent the different phases for the $d$-th dynamic signal of two antennas. After conjugate multiplication, we can see that the random phase offset has been successfully removed from the original CSI, which won't affect the capability of characterizing the human movement. The new conjugate-multiplying CSI is composed of three components, where the first component is a constant and does not change over time, and the second and the third components would change corresponding to the human target movement. Please note that in the simplified conjugate-multiplying CSI, we use the symbol $D$ to represent the number of human-introduced dynamic signals on two antennas, when modeling the relationship between conjugate-multiplying CSI and human movement, we do not make the strong assumption that human reflection is a single point reflection. Instead, in practice, the human body has multiple effective reflection points that introduce dynamic signals [2]. Among these dynamic signals, some reach the receiver directly, while others may go through the second reflection due to surrounding furniture or ceilings before reaching the receiver [3]. Using this conjugate-multiplying CSI, we will now introduce how to extract our novel metric DCM-CSI to discriminate between direct and indirect signals.

$$H_1(f,t_0+t)\cdot H_2^*(f,t_0+t) = \underbrace{A_{s_1}A_{s_2}e^{j(\phi_{s_1}-\phi_{s_2})}}_{1} + \underbrace{A_{s_1}\sum_{d=1}^{D}\alpha_d(t_0)e^{-j(\phi_d^1(t_0+t)+\phi_{s_1})}}_{2} + \underbrace{A_{s_2}\sum_{d=1}^{D}\alpha_d(t_0)e^{j(\phi_d^2(t_0+t)-\phi_{s_2})}}_{3} \quad (6)$$

Suppose there are $M$ conjugate-multiplying CSI samples within a short time window, we can construct a conjugate-multiplying vector:

$$\vec{S}(f,t_0) = [H_1(f,t_0)H_2^*(f,t_0), H_1(f,t_0+\Delta t_1)H_2^*(f,t_0+\Delta t_1), \ldots, H_1(f,t_0+\Delta t_M)H_2^*(f,t_0+\Delta t_M)],$$

where $[0,\Delta t_1,\ldots,\Delta t_M]$ is the sampling interval with respect to the sample of time $t_0$. Then by subtracting the mean value of the vector $\vec{S}(t_0)$, we can remove the constant signal term in the conjugate-multiplying CSI and get a zero-mean vector $\vec{X}(f,t_0)$:

$$\vec{X}(f,t_0) = \vec{S}(f,t_0) - \overline{\vec{S}(f,t_0)},$$

Assume variable $x(f,t_0+\Delta t_k)$ is the $k$-th element in vector $\vec{X}(f,t_0)$. Combined with Equation 6, we can express $x(f,t_0+\Delta t_k)$ as:

$$x(f,t_0+\Delta t_k) = A_{s_1}\sum_{d=1}^{D}\alpha_d(t_0)e^{j\Psi_d(t_0+\Delta t_k)} + A_{s_2}\sum_{d=1}^{D}\alpha_d(t_0)e^{j\Omega_d(t_0+\Delta t_k)}$$

Note that after the mean-subtract operation, the first static CSI part in conjugate-multiplying CSI has been removed. And $\Psi_d(t_0+\Delta t_k), \Omega_d(t_0+\Delta t_k)$ are the mean-subtract phase of dynamics signals from two antennas. Since the dynamic signals are reflected by different reflection points and go through different reflection paths, the phase changes of such signals are independent of each other. In other words, different $\Psi_d(t_0+\Delta t_k)$ are independent of each other. Similarly, different $\Omega_d(t_0+\Delta t_k)$ are independent of each other.

Then turning $x(f,t_0+\Delta t_k)$ into complex representation, it can be expressed as:

$$x(f, t_0 + \Delta t_k) = R(t_0 + \Delta t_k) + iI(t_0 + \Delta t_k)$$

$$R(t_0 + \Delta t_k) = A_{s_1} \sum_{d=1}^{D} \alpha_d(t_0) \cos(\Psi_d(t_0 + \Delta t_k)) + A_{s_2} \sum_{d=1}^{D} \alpha_d(t_0) \cos(\Omega_d(t_0 + \Delta t_k))$$

$$I(t_0 + \Delta t_k) = A_{s_1} \sum_{d=1}^{D} \alpha_d(t_0) \sin(\Psi_d(t_0 + \Delta t_k)) + A_{s_2} \sum_{d=1}^{D} \alpha_d(t_0) \sin(\Omega_d(t_0 + \Delta t_k))$$

$R(t_0 + \Delta t_k)$ and $I(t_0 + \Delta t_k)$ are the sum of two orthogonal parts, respectively. Then for each orthogonal part, it is also the sum of multiple cosine or sine functions, which can be further regarded as the sum of multiple identically distributed independent variables with zero mean. According to the Central Limit Theorem [6] , the distribution of $R(t_0+\Delta t_k)$ and $I(t_0+\Delta t_k)$ shall follow a zero-mean normal distribution $R(t_0+\Delta t_k) \sim N(0, \sigma(t_0)^2)$, $I(t_0+\Delta t_k) \sim N(0, \sigma(t_0)^2)$, where $\sigma(t_0)$ is expressed as:

$$\sigma(t_0) = \sqrt{(A_{s_1}^2 + A_{s_2}^2) \sum_{d=1}^{D} \alpha_d^2(t_0)/2 + \eta}, \tag{7}$$

where $\eta$ is the variance of Gaussian noise. **And the variance parameter $\sigma(t_0)$ is referred to as DCM-CSI, our novel metric for through-wall discrimination**. Then based on Equation 7, we can obtain the following four properties of $\sigma(t_0)$ for human sensing:

- When there is no human movement (i.e., the number of dynamic signals equals to zero), $\sigma(t_0)$ indicates the level of environmental noise and its value is small.
- $A_{s_1}, A_{s_2}$ are amplitudes of merged static signals on two antennas. In a specific environment, they are usually constant and do not change over time. For different environments, we can adjust the amplitude of each antenna by adding or subtracting a value to maintain a fixed value for $A_{s_1}, A_{s_2}$ [26].
- When a human target moves from one side of the wall to the other side, direct (indirect) dynamic signals change into indirect (direct) ones, but the overall size of $D$ remains the same.
- The amplitude $\alpha_d(t_0)$ depends on the path length of the dynamic signal and the occlusion by other objects (e.g., walls). Compared with direct signals, the amplitude of indirect signals significantly attenuates because of the wall's occlusion, which would introduce a significant change on $\alpha_d(t_0)$. After the square operation, this change will dominate $\sigma(t_0)$ and present strong distinction between direct and indirect signals.

These four properties relate the change of human-introduced dynamic signals with the change of DCM-CSI. In order to utilize DCM-CSI to differentiate direct and indirect signals, the remaining question is how to obtain $\sigma(t_0)$ from CSI. Here, we would simultaneously combine $R(t_0 + \Delta t_k)$ and $I(t_0 + \Delta t_k)$ to calculate $\sigma(t_0)$.

From previous derivation, we know that both $R(t_0+\Delta t_k)$ and $I(t_0+\Delta t_k)$ follow zero-mean Normal distributions, and share the same variance $\sigma(t_0)$. As $x(f, t_0 + \Delta t_k)$ is composed of these two independent components, the

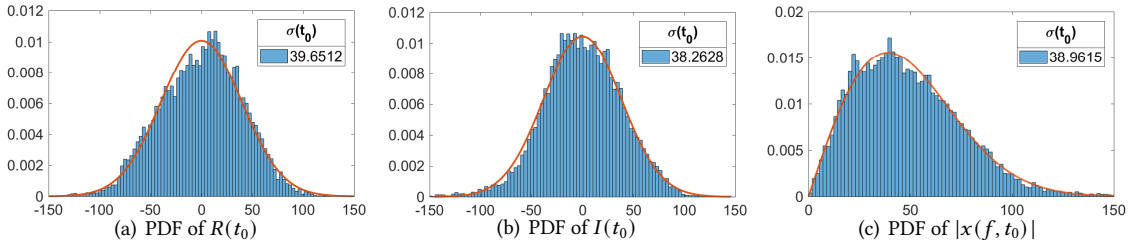


(a) PDF of $R(t_0)$ (b) PDF of $I(t_0)$ (c) PDF of $|x(f, t_0)|$

Fig. 2. Probability Distribution Function (PDF) of $R(t_0), I(t_0)$ and $|x(f, t_0)|$

absolute value of $x(f, t_0 + \Delta t_k)$ will follow a Rayleigh distribution with a parameter of $\sigma(t_0)$ [52]. To demonstrate that, we have collected 2s samples of conjugate-multiplying CSI corresponding to the dynamic signals generated by human in-situ rotation. Figure 2 shows the Probability Distribution Function (PDF) of $R(t_0), I(t_0), |x(f, t_0)|$. We can see that the distributions of $R(t_0), I(t_0)$ follow a zero-mean normal distribution with a similar variance $\sigma(t_0)$. Meanwhile, the distribution of $|x(f, t_0)|$ follows a Rayleigh Distribution with the parameter of $\sigma(t_0)$. Therefore, based on this statistical characteristic, we can obtain DCM-CSI by performing a maximum likelihood estimation of the Rayleigh distribution over the CSI samples within a time window, which can be calculated as Equation 8. In summary, by eliminating static signals and analyzing statistical characteristics of the conjugate-multiplying CSI, we are able to extract the novel boundary sensing metric from conjugate-multiplying CSI. And combined with Equation 7 and Equation 8, for the first time, we develop the mathematical relationship between human movement and DCM-CSI, and theoretically explain DCM-CSI's capability for precise boundary sensing.

$$\sigma(t_0) = \sqrt{\frac{1}{2M} \sum_{k=1}^{M} |x(f, t_0 + \Delta t_k)|^2} \tag{8}$$

## 3 EMPIRICAL STUDIES

In this section, via real-world experiments, we conduct an in-depth investigation of DCM-CSI's capability in discriminating between direct and indirect signals and demonstrate its effectiveness in precise sensing boundary determination. In the following subsections, we first study the effect of signal path length and wall blockage on DCM-CSI. Then, we compare DCM-CSI with other baseline features for direct and indirect signals discrimination. Moreover, we verify the effectiveness of DCM-CSI by testing against different types of walls. Finally, we study the impact of different antenna orientations, device locations/LoS lengths and channel settings with respect to the DCM-CSI for direct/indirect signal discrimination.

### 3.1 Influence of Reflection Path Length and Wall Blockage of Dynamic Signals

As mentioned earlier, DCM-CSI is determined by the amplitude of dynamic signals, which in turn depends on reflection path length and wall blockage. Here, we study the effect of reflection path length and wall blockage on DCM-CSI. Specifically, we first conduct experiments using the ideal reflector (a metal plate), and then turn to real setting by studying the influence of human movement.

*3.1.1 Experimental Setup.* As shown in Figure 3(a), we place a pair of Wi-Fi transceivers near the door of a bedroom with a size of 5m x 4.7m. The transceivers are placed 185cm apart from each other, both equipped with regular antennas, one for the transmitter and two for the receiver. For the ideal reflector experiments, we use a metal plate with a size of 60cm x 60cm to simulate the human movement. A sliding rail is placed at the perpendicular bisector of the transceivers. The metal plate is held by the sliding rail and controlled to move back and forth through a controlling circuit. As for the experiments of human movement, a human volunteer will walk along the bisector of the transceivers.

*3.1.2 Influence of Metal Plate Movement.* For the metal plate experiments, as shown in Figure 3(b), the sliding rail is placed across the door with one end inside the room (5m away from LoS) and the other end outside the room (2.5m away from LoS). At each 0.5m interval on the sliding rail, we vibrate the plate in-situ for 20 seconds to record the CSI data. When the metal plate is inside the room, its vibration would introduce direct signals. Once the metal plate moves outside the door, the reflection signals will become indirect due to the wall blockage. We use a sliding window of 2s to calculate DCM-CSI from CSI data. Figure 4(a) presents the resulting DCM-CSI at different locations. We can see that as the metal plate moves closer to the transceiver, the path length of dynamic signals decreases, resulting in a larger amplitude, so the value of DCM-CSI gradually increases. However, when the metal plate moves outside the door, DCM-CSI has a significant drop (at the location of -0.5m). This is because

direct signals turn into indirect signals, which are much smaller in amplitude compared with direct signals. As the metal plate continuously moves away from LoS, DCM-CSI gradually decreases due to a longer signal path length. It is noticeable that even when the plate is 5m away from LoS inside the room, the gap of DCM-CSI between direct and indirect signals is still large, indicating that it is the existence or absence of direct signals (rather than reflection path length) that dominates DCM-CSI.

*3.1.3 Influence of Human Movement .* For the human movement experiments, a volunteer walks along the bisector of the transceivers from inside the room (5m away from LoS) to LoS, and then from LoS to outside (2.5m away from LoS), stopping at each interval of 0.5m. At each stopped location, the volunteer rotates around in place for 20 seconds to record the CSI data. We use the same configuration as the metal plate experiments to calculate DCM-CSI. Figure 4(b) the DCM-CSI values obtained at each location. Compared with the results of the metal plate experiments, the DCM-CSI values of human rotation has a larger range span due to the larger displacement during human rotation process. Similar to the metal plate experiments, DCM-CSI increases gradually when the volunteer gets closer to the LoS. Once the volunteer steps outside the door, direct signals turn into indirect ones which in turn causes a drop in DCM-CSI. And for human target movement, the gap between direct and indirect signals remains clear when a person rotates even 5-meter away from LoS. Therefore, for an ordinary-sized room, our proposed metric (DCM-CSI) can be adopted to effectively determine the sensing boundary with walls for many human sensing applications.

For rooms that are much larger, such as warehouses and open-plan offices, we could place the transmitter and receiver around the sensing boundary (e.g., wall or door). Only the transition process that a target moves from one side of the boundary to the other side, could result a sudden change (rise or fall) in the DCM-CSI value as shown in Figure 4(b). In contrast, if the target stays inside the warehouse and moves to the far end of the warehouse, the value of DCM-CSI would only change gradually. Hence, by detecting the sudden rise or fall of DCM-CSI that occurs when a target crosses the boundary, we can accurately determine whether the moving target is currently located inside or outside the boundary.

## 3.2 DCM-CSI vs. Baseline Features for Discriminating between Direct and Indirect Signals

In order to sense human movement, previous works extract time-domain or frequency-domain features from raw CSI, such as variance of amplitude [43], variance of phase difference between two antennas [13, 24], or power of Doppler frequency shift [27]. Here, we compare DCM-CSI against these features in terms of discriminating between direct and indirect signals. We use the same experimental setup of transceivers as shown in Figure 3(a), and conduct experiments for both metal plate movement and human movement. The results are similar for metal

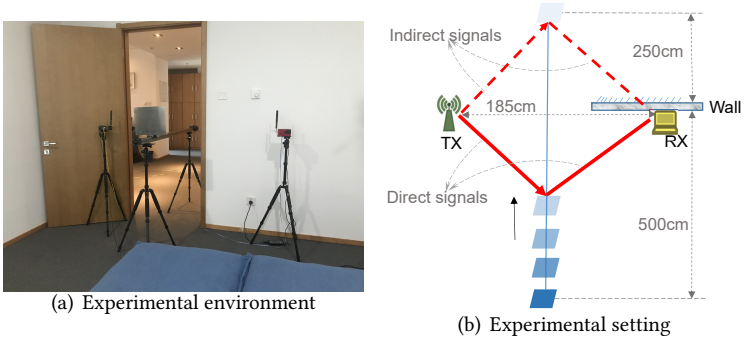


(a) Experimental environment

(b) Experimental setting

Fig. 3. Experimental setup: Influence of reflection path length and wall blockage of dynamic signals.

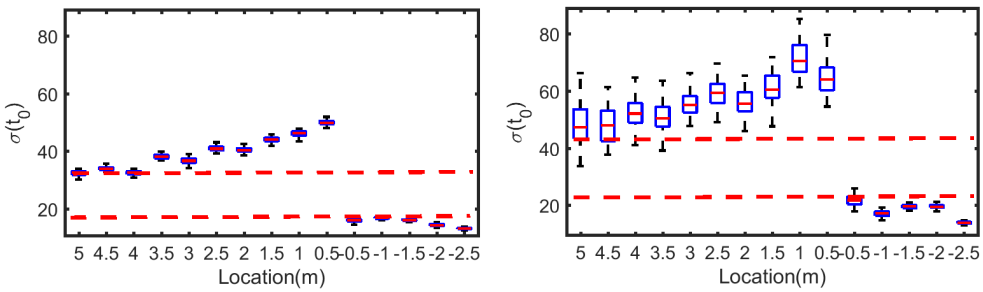


(a) Metal plate vibration at different locations (b) Human rotation at different locations

Fig. 4. Influence of signal path length and wall blockage of dynamic signals on DCM-CSI.

plate and human target. Since we focus on human sensing, here we mainly discuss the comparison results of human movement. Metal plate results are included in the Appendix.

In order to compare these features in terms of discriminating between direct and indirect signals, as shown in Figure 5, we have conducted three groups of experiments at different positions (*A*, *B*, and *C*). For each group of experiments, we collect 20 seconds of CSI data for each of three different scenarios: (1) no dynamic signal (static scenario): the sensing person is still; (2) direct signals: the sensing person is inside the room, 3m away from LoS, and rotating in-situ; and (3) indirect signals: the sensing person is outside the room, 70cm away from LoS, and rotating in-situ. For each experiment, four types of features are extracted from CSI Data: (i) standard deviation of CSI amplitude (STD of amplitude); (ii) standard deviation of CSI phase difference between two antennas (STD of phaseDif); (iii) power of Doppler frequency shift (Doppler Power); and (iv) DCM-CSI. In each group of experiments, we conduct the comparison for these features under three cases corresponding to the no dynamic signal, direct signals, and indirect signals. When utilizing STD of amplitude to sense the movement, as shown in Figure 6(a)-6(c), we can draw a threshold line for all three groups of experiments to discriminate between dynamic signals (both direct and indirect) and no dynamic signal, which shows its ability to sense human movement. However, when turn to direct and indirect signals discrimination, it presents unstable performance in different groups of experiments, where can not find a stable threshold line to discriminate between these two cases. As for STD of phaseDif and Doppler power, the results are similar with that of STD of amplitude, as shown in Figure 6(d)-6(f) and Figure 6(g)-6(i). We can draw a threshold line for these two features to discriminate between dynamic signals and no dynamic signal, but it is difficult to find a threshold line to further differentiate direct and indirect signals. This is because all of the above features either have no clear relationship with dynamic signals or are insensitive to the amplitude change of dynamic signals. DCM-CSI, unlike these features, has a clear gap between direct and indirect signals, as shown in Figure 6(j)-6(l). This indicates that we can easily find a stable threshold line to discriminate between direct and indirect signals for all groups of experiments, thus enabling us to obtain a clear sensing boundary utilizing walls.

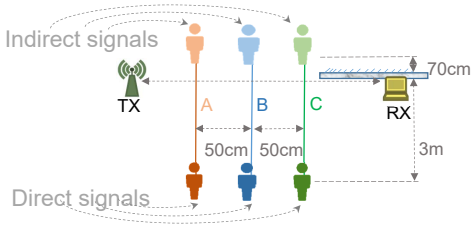


Fig. 5. Experimental setting: three different positions for metal plate movement and human movement experiments.

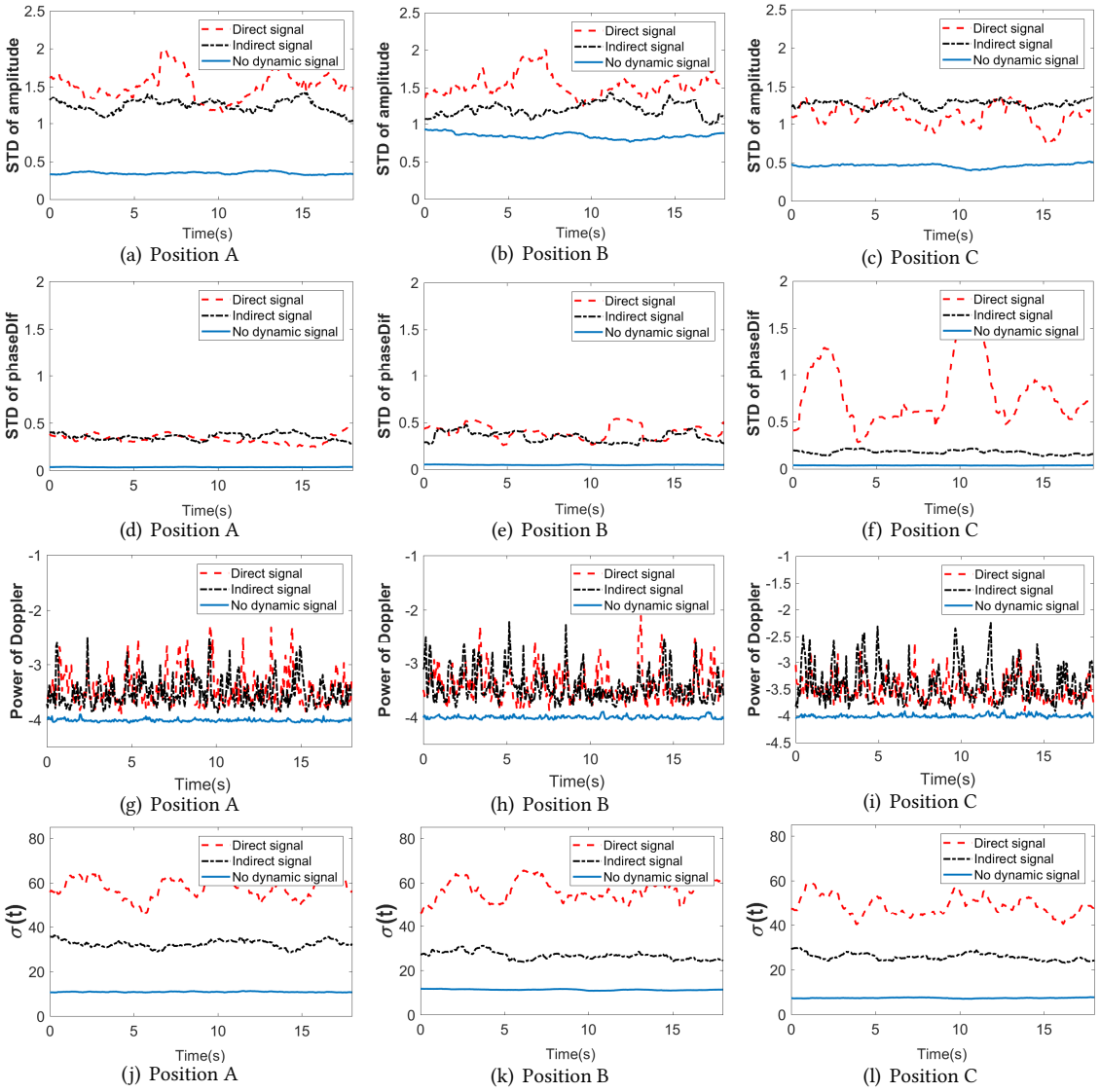


Fig. 6. Performance comparison for human movement in different groups of experiments using different features: (a)-(c) STD of amplitude; (d)-(f) STD of phase difference; (g)-(i) Power of Doppler shift; and (j)-(l) DCM-CSI.

## 3.3 Discriminating between Direct and Indirect Signals with Different Boundary Walls

In order to further study the generality of DCM-CSI in discriminating between direct and indirect signals, we conduct experiments against different walls. Among all types of walls in our daily houses, we have considered three common types [18]: exterior walls, bearing walls, and partition walls. Specifically, we study the generality of DCM-CSI in direct/indirect signals discrimination given four typical walls, including one bounding wall, one bearing wall, and two partition walls, as shown in Figure 7. One Wi-Fi transmitter and one receiver are placed in front of each wall, and are 185cm apart from each other. The experiments are also done for both metal plate and human target movement. Here we mainly discuss the experimental results of human movement. The metal plate

results are similar and are presented in the Appendix. For each of the four walls, the experimental procedure is the same as in 3.2. We also collect CSI data under three different cases (no dynamic signal, direct signals, and indirect signals). Figure 8(a)-8(d) show the obtained DCM-CSI's results for each wall. We can see that the gap between direct and indirect signals is obvious for all walls. Even for thin partition wall [31] (e.g., Partition wall2), DCM-CSI still works well for direct and indirect signals discrimination. Additionally, apart from these typical daily walls, we also study the DCM-CSI's performance with other two boundary materials: extreme thin partition wall(40mm) (Figure 7(e)) and wooden furniture (Figure 7(f)) . Correspondingly, Figure 8(e)-8(f) show the obtained DCM-CSI's results for the two types of boundary materials, respectively. Although the attenuation of the thin partition wall and wooden furniture are weaker than that of the brick wall, we can still clearly distinguish between direct and indirect signals. In summary, for most exterior walls, bearing walls, partition walls and relatively large furniture in our daily homes, DCM-CSI can generally be used to obtain a precise sensing boundary.

### 3.4 Discriminating between Direct and Indirect Signals with Different Antenna Orientations

In order to study the impact of antenna orientation on the direct/indirect signal discrimination of DCM-CSI, we conduct experiments with different antenna configurations. Due to the separation of transceivers, we take into account the antenna orientations for both transmitter and receiver. Since the antenna orientation can be vertical or horizontal, we studied all four types of antenna orientation combinations in the experiment. As shown in Figure 9, these antenna configurations include: (A) both the transmit and receive antennas are vertical; (B) both the transmit and receive antennas are horizontal; (C) the transmit antenna is vertical and receive antennas are horizontal; and (D) the transmit antenna is vertical, while one of the receive antennas is vertical and the other one is horizontal. The experimental setting is shown in Figure 10(a). For each type of antenna configuration, we collected 20 seconds of CSI data under direct and indirect signal scenarios. DCM-CSI is calculated from the collected CSI samples. The obtained DCM-CSI is illustrated in Figure 10(b). We can see clear gaps between direct and indirect signals for all antenna configurations. It is worth noting that DCM-CSI becomes smaller for antenna configurations C and D, which is the result of power loss caused by the polarization mismatch between the transmit and receive antennas [41]. However, since the gap is still clear, we can easily choose a suitable threshold for direct/indirect discrimination when utilizing different antenna configurations.

(a) Exterior wall (brick material;370mm)
(b) Bearing wall (concrete material;240mm)
(c) Partition wall1 (plasterboard material;150mm)
(d) Partition wall2 (plasterboard material;100mm)
(e) Extreme thin partition wall (single-layered plasterboard;40mm)
(f) Wooden furniture

Fig. 7. Experimental environments with different types of walls.

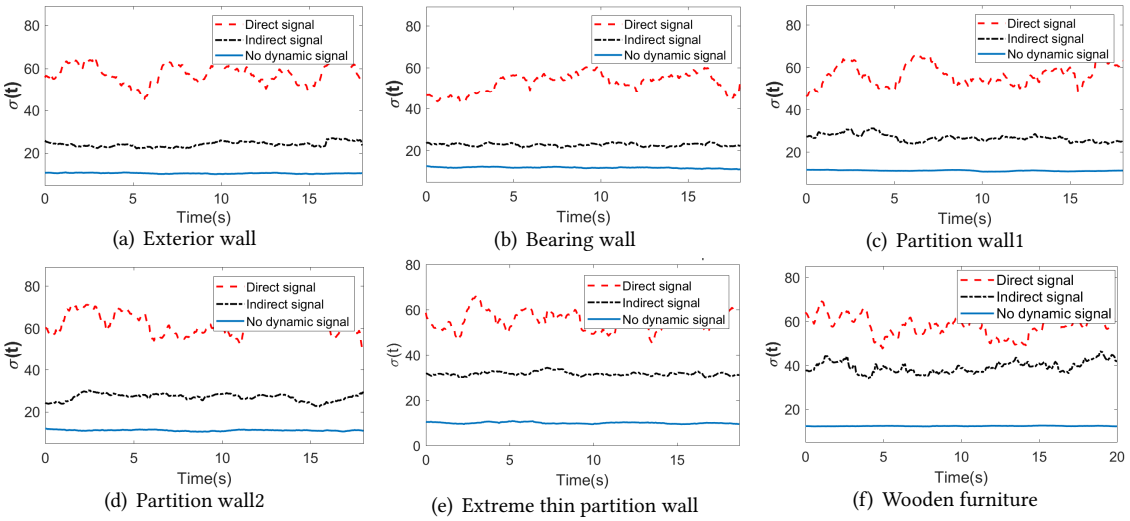


(a) Exterior wall (b) Bearing wall (c) Partition wall1

(d) Partition wall2 (e) Extreme thin partition wall (f) Wooden furniture

Fig. 8. Using DCM-CSI for direct/indirect signal discrimination for human target movement against different walls.

### 3.5 Discriminating between Direct and Indirect Signals with Different Device Locations/Distances

Apart from antenna orientation, we also studied the impact of different device locations and LoS lengths in terms of direct and indirect signal discrimination. As shown in Figure 11(a), in a typical bedroom environment, each pair of transmitter and receiver is deployed at different locations, being apart from each other with the LoS length varying from 1m to 5m. The wall on which the door is located serves as the sensing boundary. The deployment is guided by the guidelines in Section 6.1. For each pair of transceivers with a specific LoS length, we collected CSI data with the target rotating in the star-marked location (colored in red) for direct and indirect scenarios. The obtained DCM-CSI values are presented in Figure 11(b). As we can see, DCM-CSI works well for direct and indirect discrimination when transmitters and receivers are deployed at different locations along with different distances, thus demonstrating the generality of DCM-CSI for boundary sensing.

### 3.6 Discriminating between Direct and Indirect Signals with Different Channels and Sampling Rates

To further study the impact of different channels and sampling rates, we have conducted experiments to compare between 2.4GHz and 5GHz along with different sampling rates. Experiments are carried out on four kinds of channel settings: (1) 5GHz at a sampling rate of 200 packets/s; (2) 2.4GHz at a sampling rate at 200 packets/s; (3) 5GHz at a sampling rate of 2000 packets/s; and (4) 2.4GHz at a sampling rate of 2000 packets/s. The experimental

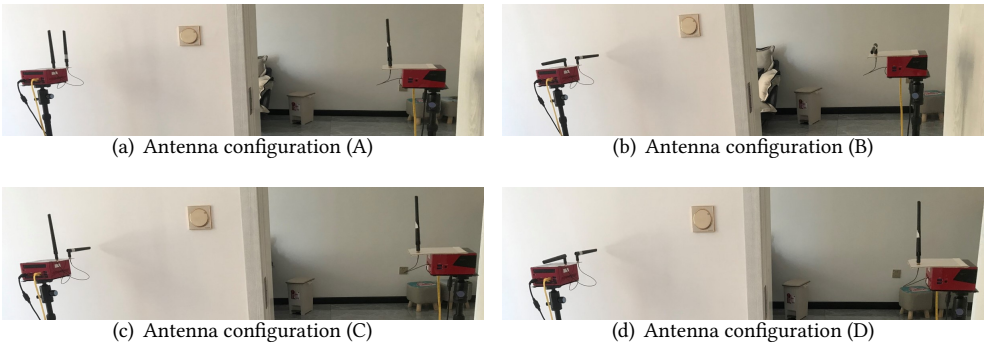

(a) Antenna configuration (A) (b) Antenna configuration (B)

(c) Antenna configuration (C) (d) Antenna configuration (D)

Fig. 9. Different antenna configurations

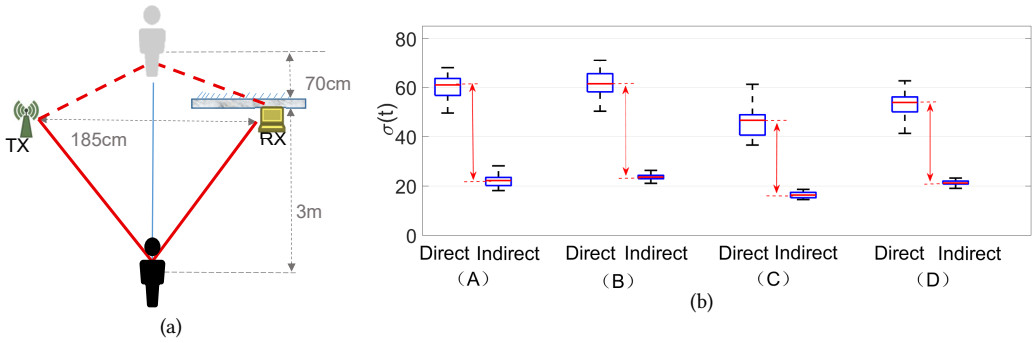


Fig. 10. (a) Experimental setup for different antenna configurations; and (b) direct and indirect signal discrimination for different antenna configurations

setup is the same as the one shown in Figure 10(a). For each kind of channel setting, CSI data are collected under the three different scenarios, including no dynamic signals, direct signals and indirect signals. Then, DCM-CSI is extracted from the collected CSI samples and the results are shown in Figure 12. We can see that the gap between direct and indirect signals is clear for all settings, which demonstrates the effectiveness of DCM-CSI under different channel and sampling rate settings.

With the experimental results above, we demonstrate the generality and effectiveness of DCM-CSI for direct and indirect signal discrimination. We believe that for many human sensing applications, DCM-CSI can be utilized to determine the sensing boundaries with daily walls. To be specific, by utilizing the significant change and related context of DCM-CSI when human target crosses a wall, we can discriminate between inside-wall and outside-wall activities, thus obtaining clear sensing boundaries with common walls. We name this DCM-CSI based sensing boundary determination method as **WiBorder**.

## 4 CASE STUDIES

Building upon WiBorder, in this section, we present two case studies. The first one is intrusion detection, a real-time system with only one pair of commodity Wi-Fi transceivers, yet still achieves high accuracy of intrusion detection. The second one is area detection, a real-time system deployed in real-life environments, which leverages one transmitter and multiple receivers to cover a larger area and more rooms.

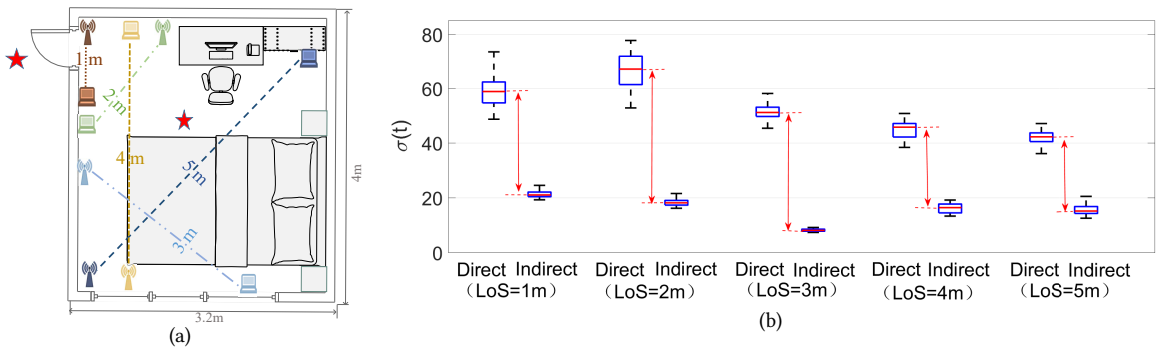


Fig. 11. (a) Experimental setup for different device locations and LoS lengths; and (b) direct and indirect signal discrimination for different device locations and LoS lengths

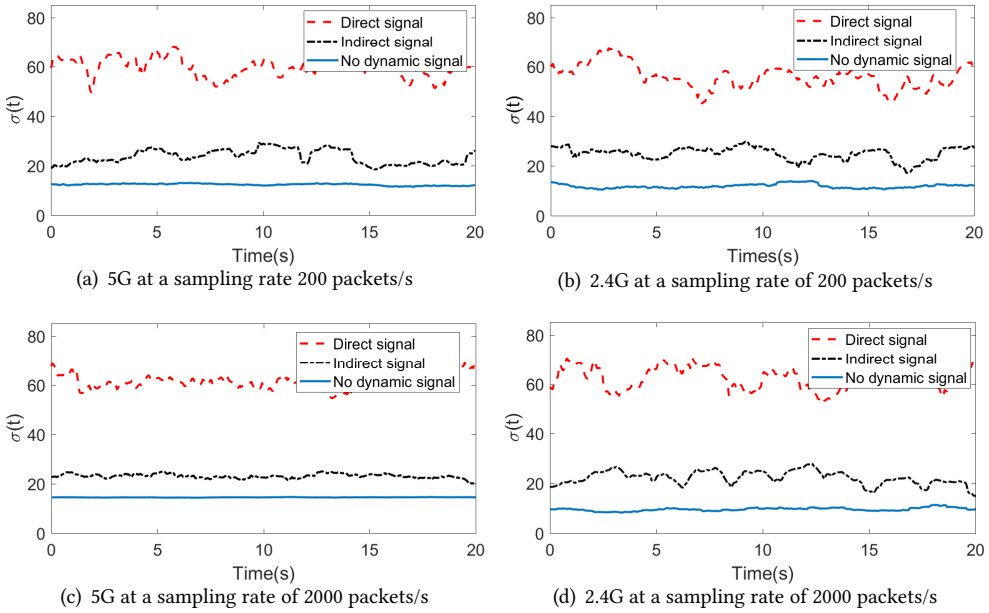


(a) 5G at a sampling rate 200 packets/s
(b) 2.4G at a sampling rate of 200 packets/s
(c) 5G at a sampling rate of 2000 packets/s
(d) 2.4G at a sampling rate of 2000 packets/s

Fig. 12. Direct and indirect signal discrimination under different channel settings

## 4.1 Case Study 1: Intrusion Detection

*4.1.1 Motivation and Targeted Intrusion Type.* Intrusion detection is critical for many smart home applications such as asset protection, home security, and eldercare. The goal is to detect whether an intruder has broken into a house or room. Many previous works [20, 50, 53, 56, 59] have attempted to address intrusion detection by detecting human motion within the coverage of Wi-Fi signals. Due to the long sensing propagation range and through-wall capabilities of Wi-Fi signals, these Wi-Fi based motion detection systems have a very large sensing range and a fuzzy sensing boundary. However, real-life intrusion detection requires accurate detection of a human target's presence within a specific area of interest, ideally drawing a clear boundary to determine whether a target has entered a monitoring area or not. Without such a clear line as the sensing boundary, when directly adopting these motion detection systems for real-word intrusion detection, motions outside the area (e.g., hallway walking) can cause lots of false alarms. Apart from avoiding these false alarms, an ideal intrusion detection system should give an alert as soon as the intrusion takes place to ensure timely reaction. In this work, we focus on the transient moment of an intruder entering the house. Leveraging WiBorder's capability of drawing a clear sensing boundary, we develop an intrusion detection system that is able to detect intrusions in a timely manner while avoiding false alarms caused by outside interference. Intrusion can happen in many different ways, and here we aim to detect the most common ways of intrusion through doors.

*4.1.2 Experimental Setup.* To build our intrusion detection system, we employ two mini-PCs equipped with cheap off-the-shelf Intel 5300 Wi-Fi cards as the transmitter and the receiver. Two antennas are attached to the receiver, and one to the transmitter. We use the CSI Tool developed by Halperin [14] to collect CSI samples on the receiver at the rate of 200 samples per second. Both the transmitter and receiver work on the 5GHz band with a 20MHz channel. To evaluate the performance of the intrusion detection system, we conduct experiments in three real-life indoor environments: a typical bedroom, an office room, and a studio in a nursing home, with the layouts shown in Figure 13. In each environment, we place the transmitter and the receiver at different corners inside the room. A web camera is deployed outside the room and points towards the door to record the ground-truth.

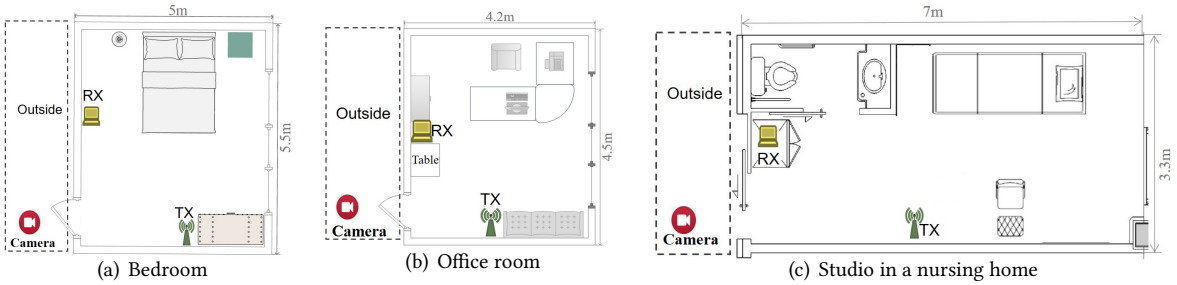


(a) Bedroom (b) Office room (c) Studio in a nursing home

Fig. 13. Experimental environments for intrusion detection.

The wall around receiver creates the difference between direct and indirect signals when the human target is inside or outside the room. Once an intruder enters the door, indirect signals will turn into direct ones, causing a significant change in DCM-CSI and indicating an intrusion event. The system simply compares the DCM-CSI with a predefined intrusion detection threshold to detect the intrusion event. All of the three environments share the same threshold value of 40 to detect intrusion.

*4.1.3 Data set and Metrics.* To fully evaluate the performance of the intrusion detection system against different individuals, we recruited 10 volunteers to perform various intrusion sessions over three weeks. These volunteers include 3 female and 7 male, aged between 20 and 38, with a height range of 155cm to 185cm, and a weight range of 49kg to 100kg. None of them had prior knowledge of our system. Each intrusion session consists of a sequence of actions. During a single session, a volunteer starts from outside the room, freely performing any activities such as walking, running, or jumping before crossing the door and entering the room in whatever manner he/she likes. Then, after walking in the room for a while, he/she leaves the room and walks away. The whole session lasts for about 30 to 50 seconds, and the entire process is recorded by the pre-deployed camera. During all experiments, we deliberately kept the door open and let other people pass by to further test the robustness of our system. In total, we have collected **1,324** sessions, which consist of 1,324 intrusion events and 1,324 cases of outside activities. In order to synchronize the ground-truth video with the CSI samples, the transmitter's program outputs a timestamp every 0.2s when transmitting the CSI data. Both the timestamp and ground-truth video are recorded in an auxiliary video file by the screen recorder. An example is shown in Figure 14, where each frame of the auxiliary video consists of a screenshot of the video stream and the CSI timestamp stream. Therefore, for each intrusion instance, we can check the video file to obtain the corresponding timestamp of the CSI data, thus achieving synchronization between the CSI data and ground-truth video. Moreover, we have drawn a marked line at the door frame to help us obtain the ground-truth timestamp when a target crosses the line to enter the room. We use a sliding window of 2s to calculate the DCM-CSI. The sliding window slides at a step size of 0.05s, so we can make an intrusion decision every 0.05s. And in order to fully evaluate our intrusion detection system, we use TPR and FPR to respectively quantify intrusion detection rate and false alarm rate as shown in Figure 15.


Fig. 14. An example frame of auxiliary video for synchronization

$$TPR = \frac{\#\ of\ correctly\ detected\ times\ of\ intrusion}{\#\ of\ times\ of\ intrusion\ that\ are\ actually\ performed}$$

$$FPR = \frac{\#\ of\ mistakenly\ detected\ times\ of\ intrusion}{\#\ of\ times\ of\ outside\ door\ activities\ that\ are\ actually\ performed}$$

Fig. 15. Metrics for evaluation

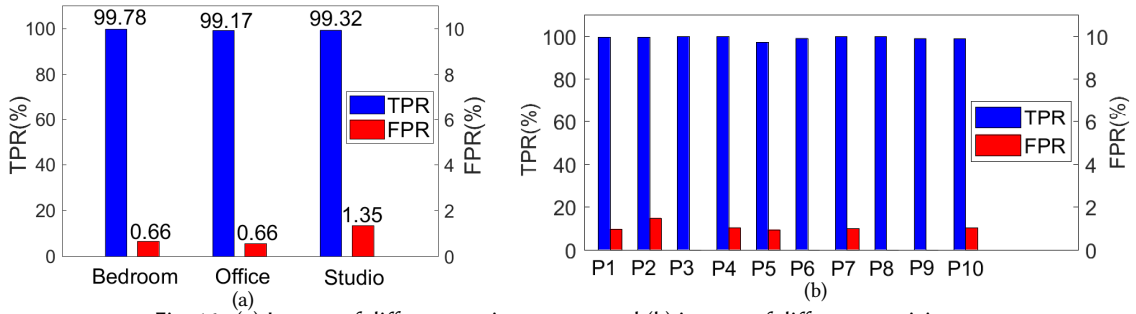


Fig. 16. (a) Impact of different environments; and (b) impact of different participants (only intrusion alarms reported within 1s are considered valid).

*4.1.4 Evaluation.* Our intrusion detection system achieves an overall accuracy of 99.4% TPR and 0.68% FPR for all intrusion sessions. To be specific, in terms of the system's missed reports (100%-99.4%), all of the 1,324 intrusion events are detected by our system. There exist missed reports only because their detection delay is more than 1s, which are regarded as unsuccessful reports. As for reported false alarms (0.68%), they only come from the large-scale activities when the target jumps or runs strenuously outside but near the door, which might cause a significant change of DCM-CSI exceeding the detection threshold. For small-scale activities, the DCM-CSI change is very small due to a relatively small amount of direct signals. Thus, small-scale activities will not introduce any false alarms. In conclusion, thanks to our robust boundary determination scheme, we eliminate almost all missed alarms and false alarms, and achieve high TPR and low FPR at the same time, which advances real-life deployment of Wi-Fi based intrusion detection system.

**Impact of different environments.** To further evaluate the robustness of our system against different environments, we compare experimental results in three different indoor environments, and show the TPR and FPR of each environment in Figure 16(a). We can see that our system achieves good performance for all three environments. And it is worth noting that all of the three environments share the same detection threshold value of 40, which means that this threshold value is robust and insensitive to environmental changes.

**Impact of different participants.** Since different people have different shapes and gait styles, the way they intrude a room could be different. Here, we also evaluate the robustness of our system against individual diversity. The system performance of different participants are shown in Figure 16(b). We can see that, for different volunteers, our intrusion detection system can achieve higher than 97% TPR and lower than 2% FPR. This indicates that our system can maintain high performance on different intruders.

**Impact of tolerated detection delay.** We also study the impact of different tolerated detection delay on our system performance. Since a false alarm is counted whenever a non-intrusion activity is incorrectly reported as an intrusion, FPR is not affected by the detection delay. Thus, only TPR is influenced by such tolerated detection delay. We tested our system against different tolerated decision delay from 0.4s to 2s with a step size of 0.2s, and the results are shown in Figure 17. It shows that the greater tolerated delay, the better performance of our system

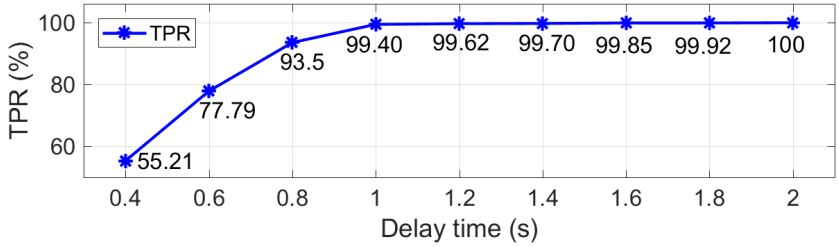


Fig. 17. Impact of tolerated detection delay (100% TPR achieved when delay is more than 2s).

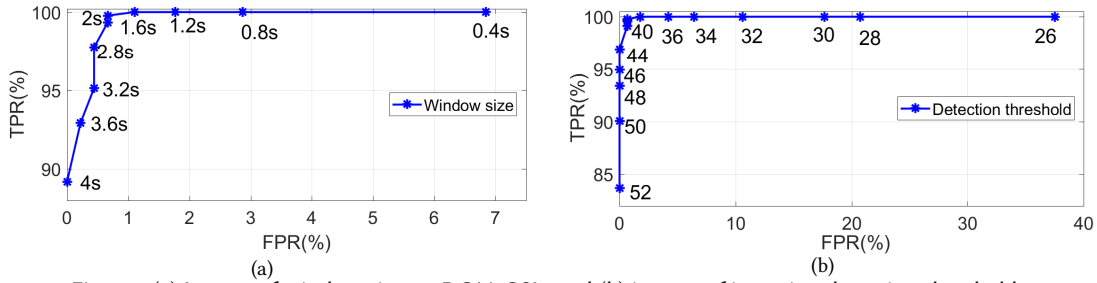


Fig. 18. (a) Impact of window size on DCM-CSI ; and (b) impact of intrusion detection threshold.

achieves. When the tolerated detection delay is greater than 2s, our system achieves a TPR of 100% for intrusion detection, which means we did not miss any intrusion action. In our system, considering the tradeoff between timeliness and TPR, we set 1s as the tolerated detection delay.

**Impact of window size for DCM-CSI calculation.** Since DCM-CSI is calculated from CSI samples collected within a time window, its value is related to the window size. We used the window size of 2s to present results discussed above, and here we evaluate the impact of different window size on system performance. Figure 18(a) shows the ROC curve of the system performance for different window sizes ranging from 0.4s to 4s with a step size of 0.2s. As the window size increases from 0.4s to 2s, the TPR of our system is stable and the FPR gradually decreases, indicating fewer false alarms and better performance. A sliding window with a larger window size contains more CSI samples and thus can better represent the statistical characteristics of DCM-CSI, resulting in a more accurate DCM-CSI value. Furthermore, a larger sliding window for calculating DCM-CSI is able to average out abnormal CSI samples and thus reduce the impact of environmental noises. When the window size continually becomes larger more than 2s, although the FPR gets better, the TPR of intrusion detection starts to get worse. That is because too large window size will cause an increase in the delay of intrusion detection. With more intrusion events detected after one second, the TPR of the system will gradually decrease. In the current setting, we choose a window size of 2s for intrusion detection. Other applications can certainly adjust this size to meet their needs.

**Impact of intrusion detection threshold.** To detect intrusions, we have utilized a threshold to discriminate between inside activities and outside activities. Here, we also vary this threshold from 26 to 52 to study its impact on system performance. As shown in Figure 18(b), when the threshold value is small, the system maintains high TPR and FPR. As the threshold becomes larger, both TPR and FPR decreases. In general, the system achieves better performance with both high TPR and low FPR, when the threshold value lies within the interval [35-45]. Here, we choose 40 as the intrusion detection threshold value for our system.

## 4.2 Case Study 2: Area Detection

*4.2.1 Experimental Setup.* Based on WiBorder, we further built an area detection system, and deployed it in two different environments: a studio in a nursing house and a smart home. As shown in Figure 19(a) and Figure 19(d), the nursing studio has three areas: bathroom, hallway, and bedroom; and the smart home has four areas: bedroom, bathroom, living room, and kitchen. In order to achieve accurate area detection, we deployed one transmitter and several receivers in each environment with one receiver per area and placed around the corner. The GUI of our systems for the two environments are shown in Figure 19(b) and Figure 19(e), respectively.

*4.2.2 Multi-Device Fusion.* Recall that direct signals are defined as the signals that are directly reflected by a moving target when propagating from a transmitter to a receiver. Indirect signals are the ones that are reflected by a moving target but penetrated through walls along their propagation. When the human target switches between different areas, the direct/indirect signals' situations are different due to different conditions of wall blockage.

By taking advantage of these differences, we are able to extract DCM-CSI metrics from all receivers and obtain global knowledge about the human target's area. We encode the situations of having indirect or direct signals by assigning 0 or 1 to each receiver. We also define a set of valid state transition encoding that trigger the area state updates. In other words, the system updates its area state only when the current encoding gathered from different receivers matches one of the defined valid transition encoding. Otherwise, the system remains in its previous area state. Take the smart home as an example (i.e., Figure 19(a)), we depict its Area-Transition-Diagram for better illustration, as shown in Figure 19(f). Suppose a sensing target who is inside the living room, wants to enter the bedroom. The target needs to move close to the bedroom door (i.e., the boundary between the living room and the bedroom). As shown in Figure 20(a), when he/she gets close to the door but is still outside the bedroom, RX3 and RX4 receive direct signals, while other devices receive indirect signals. For this scenario, the state encoding can be represented as (RX1=0,RX2=0,RX3|RX4=1,RX5=0) (i.e., 0010) where "|" refers to "or". Right after he/she crosses the door and enters the bedroom, no direct signals reach RX3 or RX4 due to the blockage of the bedroom walls. Only RX1 receives direct signals as shown in Figure 20(b). The current state encoding becomes (RX1=1,RX2=0,RX3|RX4=0,RX5=0) (i.e., 1000). Since such a new encoding matches one entry of our defined transition encoding, the system is triggered to update the area state of the sensing target as "inside

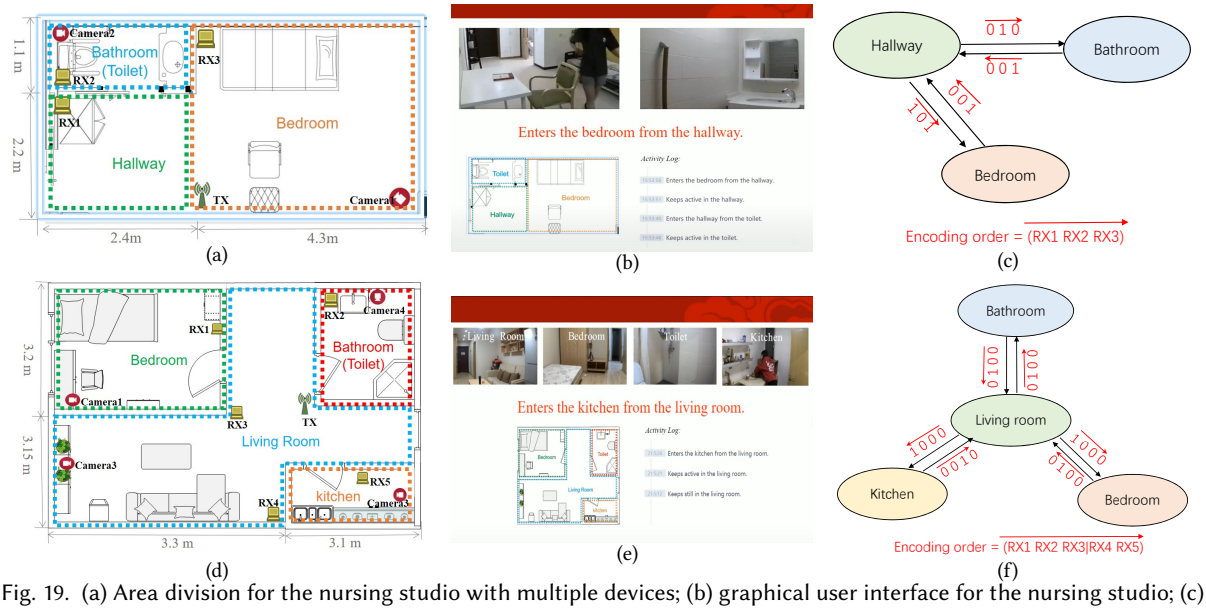


Fig. 19. (a) Area division for the nursing studio with multiple devices; (b) graphical user interface for the nursing studio; (c) Area-Transition-Diagram for the studio; (d) area division for the smart home with multiple devices; (e) graphical user interface for the smart home; and (f) Area-Transition-Diagram for the smart home.

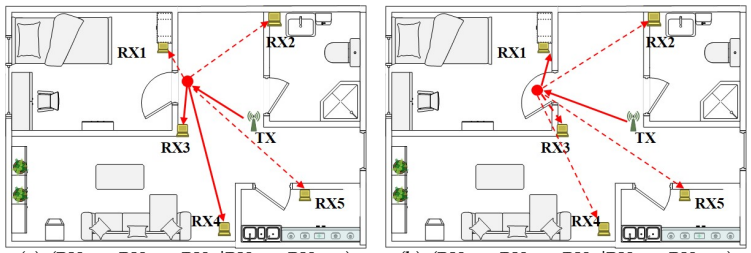


Fig. 20. Direct and indirect signal encodings at different locations

| Actual Area \ Predicted area | Bath-room | Hallway | Bedroom |
|---|---|---|---|
| Bath-room | 0.981 | 0.019 | 0 |
| Hallway | 0.018 | 0.953 | 0.029 |
| Bedroom | 0 | 0.026 | 0.974 |

(a) Confusion matrix for studio

| Actual Area \ Predicted area | Bath-room | Living Room | Bed-room | Kitchen |
|---|---|---|---|---|
| Bath-room | 0.975 | 0.025 | 0 | 0 |
| Living Room | 0.015 | 0.952 | 0.022 | 0.011 |
| Bed-room | 0 | 0.023 | 0.977 | 0 |
| Kitchen | 0 | 0.020 | 0 | 0.980 |

(b) Confusion matrix for smart home

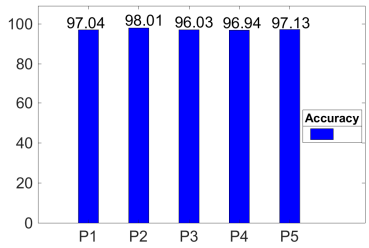


(c) Accuracy of different participants

Fig. 21. Performance of the area detection system.

the bedroom". If the target walks to the bed, then lies on the bed and stays still, the state encoding becomes (RX1=0,RX2=0,RX3|RX4=0,RX5=0) (i.e., 0000) since there are no dynamic signals. As “0000" does not match any transition encoding we defined, the system will remain in the area state of “inside the bedroom". Therefore, the area state is updated right after the target crosses the boundary, while the motions taken inside an area does not trigger any state updates. Similarly, in a complex area with multiple corners, before the target reaches the corner, the system has been updated to the correct area state when he/she crosses the boundary. Thus, using the Area-Transition-Diagram, we are able to accurately determine a human target's area once we have gathered 0/1 encoding from all receivers.

*4.2.3 Data Set.* To evaluate the performance of our system, for each environment, we have asked 5 volunteers to conduct daily activities for an aggregated duration of 1200 minutes. We collected 12 sets of activities for each volunteer, and each lasts for about ten minutes. During each set, a volunteer can freely switch between different areas, or perform various activities in each area, such as going to bed in the bedroom, putting clothes on/off in the hallway; washing hands in the bathroom, watching TV in the living room, etc. To fully evaluate the system, the volunteers are advised to switch between areas as much as possible. In total, there are 4390 times of area switches in the 1200 minutes. A synchronized ground-truth video stream is recorded for each set of activities. For every 0.05s, our system will output a line of text describing the human area state, and at the same time, records the result to a log file. Thus, for each set of data, we have a result log file corresponding to the whole process.

*4.2.4 Evaluation.* The system performance of area detection in two environments are presented in the form of confusion matrix, as shown in Figure 21(a) and Figure 21(b), respectively. Element $p_{i,j}$ represents the percentage of time when the human target is in fact in area $i$ but being estimated in area $j$. It is worth noting that there is a transition area in each environment, through which one must pass before reaching another area, e.g., hallway in nursing studio and living room in smart home. In the presence of transition areas, we know that the human target is not able to switch directly between bedroom and bathroom/kitchen. Thus, from the confusion matrix, we notice that all the mistakes are caused by switches between adjacent areas. Since an area state update is triggered by the predefined state transition encoding, the system only updates the area state right after the target crosses a boundary (i.e., switch between adjacent areas). Activities inside each area will not trigger any update and therefore will not cause false alarms. The false alarms merely come from the delay of area state update when the target switches between adjacent areas. As the hallway and living room are both transition regions in the two environments, they suffer from delays in both hallway (living room)–bedroom and hallway (living room)–bathroom switches. Hence, their accuracy is slightly lower than that of the other areas. Apart from the evaluation of different environments, we also evaluated our system against individual diversity, and the system performance holds consistency for different individuals as shown in Figure 21(c). Overall, our system achieves a good area detection accuracy of up to 97.03%.

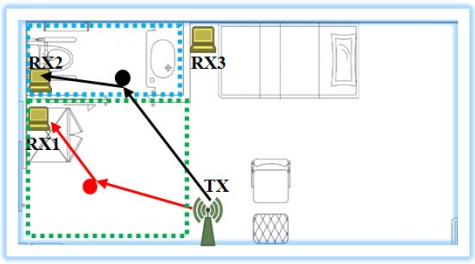


Fig. 22. Two people in two different areas.

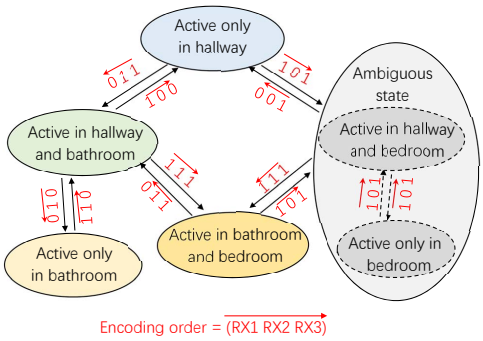


Fig. 23. Area-Transition-Diagram for Multi-area Tracking.

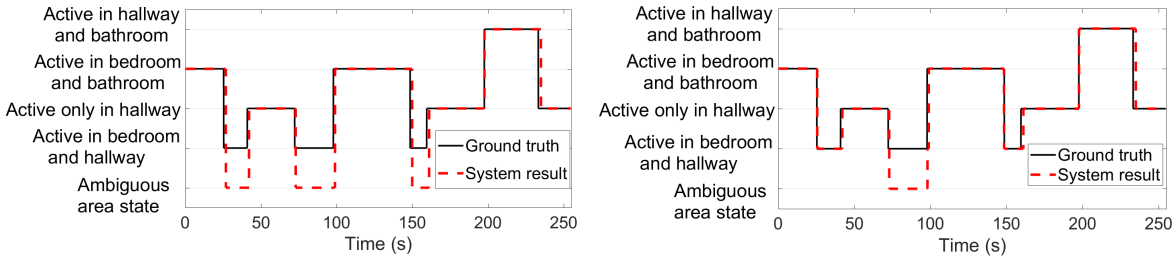


Fig. 24. Area detection results for two people: without (left) or with (right) high-level semantics.

*4.2.5 Feasibility Study of Multi-area Tracking of Active People.* The experiments above have shown that our area detection system achieves good performance when determining a single target's area. When more than one people are active in different areas at the same time, our system can also provide their area information, thus enabling multi-area tracking. Taking two persons for example, assume one person is active inside the bathroom, and the other one is in the center of the hallway, as shown in Figure 22. The person in the hallway would introduce direct signals on RX1 but indirect signals on RX2 and RX3. Meanwhile, the person in the bathroom would introduce direct signals on RX2 but indirect signals on RX1 and RX3. Since for each receiver, the power of received direct signals greatly surpasses (i.e., dominates) the power of received indirect signals, we can encode the current direct/indirect situations of the three receivers as (1,1,0). Likewise, we can depict the Area-Transition-Diagram for multi-area tracking as shown in Figure 23. To validate, we asked two volunteers to perform daily activities for 250 continuous seconds, and obtained the multi-area tracking results based on the encoding table above, as shown in Figure 24(a). There is some ambiguity in the figure between two situations: (1) when both people are active in the bedroom and (2) when one is active in the hallway and the other one is active in the bedroom. This is because they share the same transition encoding. Such ambiguous area states can be further eliminated by utilizing more devices or combining high-level context information. For example, since a person cannot move directly from the bathroom to the bedroom, the state of one person in the bedroom and the other in the bathroom cannot directly turn into the state of both people in the bedroom. Therefore, coupling with this context, our system can correct the first and third ambiguous states, as shown in Figure 24(b). In summary, based on WiBorder, our area detection system shows its potential in multi-area tracking for multiple active persons. Although further research is needed, our work is one step further towards addressing the challenging multi-user sensing problem.

## 5 RELATED WORK

In recent years, various human sensing techniques have been developed, including inertial sensors-based [5, 49], camera-based [32, 34], sound-based [8, 44, 55], visible-light based [17, 22], ambient-sensors based [16, 30, 37], RFID-based [29, 46], Infrared-based [19, 57] and Radar-based [2–4, 9–11] approaches. Inertial sensor-based methods require the target to carry or wear a special-purpose device for sensing. Camera-based technologies may raise privacy concerns and do not work well under poor lighting conditions. Sound-based techniques are vulnerable to acoustic noise and have limited coverage. Visible light methods can only be applied in line-of-sight scenarios. Ambient sensor-based solutions usually require dense deployment, which incurs higher cost for both installation and maintenance. Infrared-based sensing systems can be utilized to achieve the boundary sensing by deploying multiple transceiver pairs at key entrances. Instead of utilizing multiple transmitters, Wi-Fi based systems only require one transmitter and multiple receivers. Moreover, those Wi-Fi devices can be also utilized to support other sensing applications, such as respiration detection [28, 58, 60], gesture recognition [23],activity recognition [7, 15, 40, 43, 45], etc. UWB radars are dedicated devices with much higher cost than Wi-Fi transceivers. It's true that UWB radars can achieve high-precision localization and boundary crossing detection. However, due to the limited sensing range and angle, each UWB radar needs to face towards the targeted sensing boundary in order to achieve precise boundary determination. For multi-boundary determination or supporting more sensing applications (e.g., activity recognition), multiple UWB radars need to be deployed in order to cover the entire home, leading to much higher cost. Different from UWB radars, Wi-Fi devices are ubiquitous for communication in home environments. Various Wi-Fi-enabled home appliances (e.g., router, TV, refrigerator) could be reused to support various applications such as boundary sensing. Next, we focus on device-free human sensing using commodity Wi-Fi devices and discuss Wi-Fi based works that are most relevant.

### 5.1 Device-free Human Motion Detection using Wi-Fi

Wi-Fi signal has been used to detect human motion within the coverage of Wi-Fi devices, and a number of techniques have been proposed. Depending on the features extracted from Wi-Fi signal, these techniques can be categorized as time-domain or frequency-domain based methods. Time-domain based methods extract features such as the variance or correlation of Wi-Fi signal to detect human motion. For example, earlier solutions detect human motion using the variance of RSSI [20, 56]. CARM [43] employs variance of CSI amplitude to detect motion for activity recognition. FIMD [53] and WiDetect [59] utilize correlation of CSI amplitude over time for motion detection. PADS [36] combines both the phase and amplitude information of CSI to improve motion detection accuracy. DeMan [50] not only detects human motion but also detects the existence of a still human based on respiration sensing. MoSense [13] and AR-Alarm [24] utilize variance of the phase difference for human motion detection. As human motion introduces Doppler effect on Wi-Fi signal, it can be detected by capturing this Doppler effect in the frequency domain. WiVit [27] utilizes power of Doppler frequency shift as the feature to effectively detect human motion.

All of these methods aim to detect human motion within the sensing range of Wi-Fi devices. Due to the long propagation range of Wi-Fi signals [48], Wi-Fi based sensing systems have a very large sensing range and a fuzzy sensing boundary. However, in real life, Wi-Fi based human sensing applications usually require accurate detection of a human target's presence within a given area of interest, ideally drawing a clear line to determine whether a human target has entered a sensing area or not. Without such a clear line as the sensing boundary, inference from outside the area of interest can cause lots of false alarms. Therefore, instead of focusing on human motion sensing in a fuzzy range, our work aims to determine a clear Wi-Fi based sensing boundary using common walls, which is orthogonal to current Wi-Fi based human sensing applications and in fact makes these applications feasible in the real world by defining a specific sensing area of interest.

### 5.2 Device-free Human Localization using Wi-Fi

Wi-Fi signal has also been used to achieve device-free human localization in indoor environments. Since the concept of device-free localization was first introduced in 2007 [56], many device-free localization systems have been proposed, which can be categorized as fingerprinting-based methods and geometric mapping-based methods. Among the fingerprinting-based methods, Nuzzer [39] and Ichnaea [38] use RSSI signature as the fingerprint for device-free localization. Pilot [54] and MonoPHY [1] systems employ finer CSI information as the fingerprint to improve accuracy. LiFS [42] utilizes the Fresnel model to improve the accuracy of localization when the target is on the LoS path of the transceivers. Although these approaches work well when the human target is stationary, they face a great challenge in dealing with moving targets. Geometrical mapping-based methods, such as Dynamic-MUSIC method [25] and IndoTrack system [26], employ the Angle-of-Arrival (AoA) information to locate and track the target. WiDar [35] tracks a target based on the amplitude of Doppler frequency shift with multiple devices. SiFi [12] utilizes only one AP with multiple antennas to locate the target. However, all these works require the communication link of LoS propagation to reduce the fluctuations of signal feature. Although much progress has been made in the field of Wi-Fi LoS identification [51, 61], the 90th percentile error of state-of-the-art device-free human localization solutions is still as high as 2m [12]. Rather than obtaining inaccurate location information, our work aims to solve the critical problem of accurately determining whether a human target has crossed a specific boundary line and entered an area of interest.

## 6 DISCUSSION

In this work, we propose WiBorder, a method for accurate Wi-Fi sensing boundary determination, which can be applied to state-of-the-art Wi-Fi sensing applications. In this section, we first introduce some deployment guidelines for those Wi-Fi sensing applications which require a clear sensing boundary in their implementation. Then we briefly discuss several directions for future research.

### 6.1 Deployment Guidelines

The existence of walls plays an important role in WiBorder, and actually, it is the blockage of Wi-Fi signals by walls that enables WiBorder to achieve two-side discrimination. Specifically, the sensing boundary we define in this paper is shaped by the line formed by the location of the RX and the endpoint of the partial wall or objects. For different layouts in different environments, the signal blockage condition usually differs. As such, we need some guidance in terms of where to place the Wi-Fi transceivers given specific indoor layout and sensing

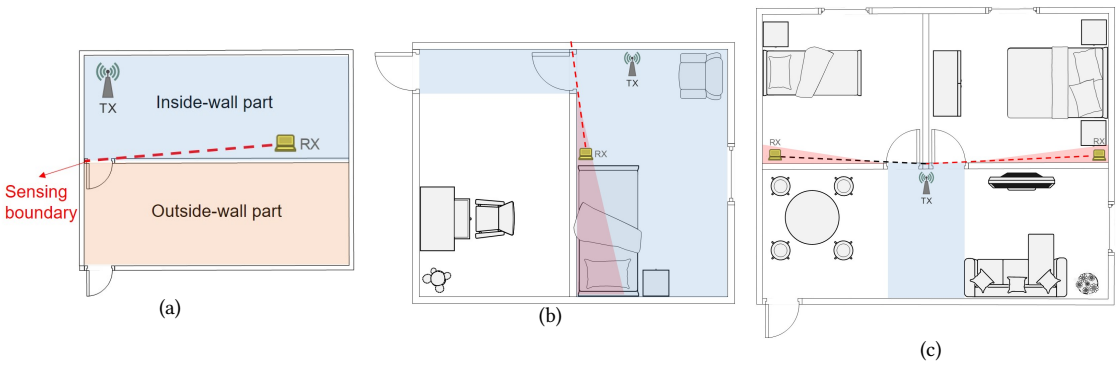


Fig. 25. (a) Space division when the wall is leveraged as a sensing boundary; (b) transceivers deployment for single-boundary determination: blue area for transmitter deployment and red area for receiver deployment; and (c) transceivers deployment for multiple-boundary determination: blue area for transmitter deployment and red area for receivers deployment.

demand, either theoretically or empirically. We have developed two guidelines for WiBorder deployment, which are illustrated by a simple example in Figure 25(a). Assume a space is divided by a common wall into two parts: inside-wall space and outside-wall space, wherein the inside-wall space serves as the target sensing area. Then, in order to leverage the wall or its extensions as a sensing boundary, one can deploy Wi-Fi transmitters and receivers according to the following two guidelines:

(1) The Wi-Fi receiver is preferably deployed in the inside-wall space and not visible by a human target in the outside-wall space.
(2) The Wi-Fi transmitter can be deployed either in the inside-wall space or outside-wall space, but it should be visible by a human target when he gets into the inside-wall space.

Based on the above guidelines, we can quickly select the appropriate places to deploy the transmitter and receivers, as shown in Figure 25(b), colored in blue and red. As for multi-room houses, WiBorder is also able to achieve multiple-boundaries determination based on these two guidelines. As shown in Figure 25(c), by reasonably deploying one transmitter and multiple receivers, the multiple boundaries can be formed by multiple walls in the house. When it comes to the case that the LOS between a user and both the TX and RX is blocked by a object (e.g, the sofa is moved in front of the TX in Figure 25(b)), one can make some minor deployment adjustment to satisfy the deployment guidelines (e.g., place the TX in front of the sofa). Therefore, as long as deployment guidelines are satisfied, we can always effectively detect the boundary crossing event when he/she enters the room.

### 6.2 Supporting Activity Recognition Systems

Besides the application of intrusion detection and area detection, WiBorder can also provide valuable context information for activity recognition systems. For example, in our daily life, sleeping always happens in the bedroom, whereas cooking usually happens in the kitchen. We can use area information reported from WiBorder to help reducing the training size of such systems, since once we have the area information, we can greatly reduce the classification complexity and improve recognition accuracy. Therefore, how to develop an activity recognition system based on WiBorder is also worthy of future investigation.

### 6.3 Boundary Materials

In this work, we have demonstrated that DCM-CSI can be generally used to obtain a precise sensing boundary for most exterior walls, bearing walls and partition walls in our daily homes. But for extremely thin or transparent materials, such as glass partition, it is not as effective. This limitation is due to the weak attenuation effect of these materials, and electromagnetic waves can easily pass through them. For these materials, one could jointly utilize relatively large furniture (e.g., wooden bookcase) to act as a boundary. In the future, we plan to investigate more materials and study the capability of DCM-CSI for boundary sensing under various scenarios.

### 6.4 Multi-person Sensing

Passive or device-free sensing of multiple persons is a well-known challenging problem. Although our area detection system shows its potential in multi-area tracking for multiple active persons, further research is needed for multi-person sensing. When there are multiple targets, each non-still target will generate multiple dynamic signals to the receiver, so the signal received at the receiver is a superposition of multiple targets. Due to the small Wi-Fi bandwidth (20MHz), it is extremely difficult for commodity Wi-Fi devices to separate these reflected path signals and obtain the accurate number of targets. Area trajectory matching of different sensing targets is also challenging. This is an important direction for our future work.

## 7 CONCLUSION

Contactless sensing with pervasive Wi-Fi signal is a promising sensing approach in our daily lives. In real-life environments, a lot of Wi-Fi based sensing applications require prior knowledge of the human's presence in the sensing area of interest. However, no prior solution exists to accurately determine whether a person has entered a given area (i.e., no precise boundary sensing), which severely limits real-life adoption of these Wi-Fi based sensing applications. In this paper, for the first time, we propose a precise Wi-Fi based sensing boundary determination method, i.e., WiBorder, which leverages common walls in our daily life. WiBorder first applies conjugate multiplication between two antennas' CSI readings, which effectively eliminates the time-varying phase offset in the raw CSI, and at the same time amplifies through-wall signal amplitude attenuation. By analyzing the theoretical relationship between human movement and conjugating-multiplying CSI, we propose a novel metric (DCM-CSI), which enables WiBorder to achieve through-wall signal discrimination. Finally, to demonstrate the effectiveness of WiBorder, we have developed two case studies for real-life scenarios: (1) an intrusion detection system that achieves 99.4% intrusion detection rate and 0.68% false alarm rate; and (2) an area detection system that achieves 97.03% area detection accuracy. Moreover, we have conducted a feasibility study of multi-area tracking, which shows WiBoarder's potential in providing useful location information for multi-person sensing. WiBorder can be a core and fundamental function module for many Wi-Fi based indoor sensing applications.

## ACKNOWLEDGMENTS

This research is supported by National Key Research and Development Plan under Grant No.2016YFB1001200, Project 2019BD005 supported by PKU-Baidu Fund, and Peking University Information Technology Institute (Tianjin Binhai).

## REFERENCES

[1] Heba Abdel-Nasser, Reham Samir, Ibrahim Sabek, and Moustafa Youssef. 2013. MonoPHY: Mono-stream-based device-free WLAN localization via physical layer information. In *2013 IEEE Wireless Communications and Networking Conference (WCNC)*. 4546–4551.

[2] Fadel Adib, Chen-Yu Hsu, Hongzi Mao, Dina Katabi, and Frédo Durand. 2015. Capturing the Human Figure through a Wall. *ACM Trans. Graph.* 34, 6, Article 219 (Oct. 2015), 13 pages.

[3] Fadel Adib, Zach Kabelac, Dina Katabi, and Robert C. Miller. 2014. 3D Tracking via Body Radio Reflections. In *11th USENIX Symposium on Networked Systems Design and Implementation (NSDI 14)*. Seattle, WA, 317–329.

[4] Boyd Anderson, Mingqian Shi, Vincent Y. F. Tan, and Ye Wang. 2019. Mobile Gait Analysis Using Foot-Mounted UWB Sensors. *Proc. ACM Interact. Mob. Wearable Ubiquitous Technol.* 3, 3, Article 73 (Sept. 2019), 22 pages.

[5] Agata Brajdic and Robert Harle. 2012. Scalable indoor pedestrian localisation using inertial sensing and parallel particle filters. In *2012 International Conference on Indoor Positioning and Indoor Navigation (IPIN)*. 1–10.

[6] Richard Hedley Clarke. 1968. A statistical theory of mobile-radio reception. *The Bell System Technical Journal* 47, 6 (July 1968), 957–1000.

[7] Zhang Daqing, Wang Hao, and Wu Dan. 2017. Toward Centimeter-Scale Human Activity Sensing with Wi-Fi Signals. *Computer* 50, 1 (2017), 48–57.

[8] Thilina Dissanayake, Takuya Maekawa, Daichi Amagata, and Takahiro Hara. 2018. Detecting Door Events Using a Smartphone via Active Sound Sensing. *Proc. ACM Interact. Mob. Wearable Ubiquitous Technol.* 2, 4, Article 160 (Dec. 2018), 26 pages.

[9] D. P. Fairchild and R. M. Narayanan. 2016. Multistatic micro-doppler radar for determining target orientation and activity classification. *IEEE Trans. Aerospace Electron. Systems* 52, 1 (2016), 512–521.

[10] O. R. Fogle and B. D. Rigling. 2012. Micro-Range/Micro-Doppler Decomposition of Human Radar Signatures. *IEEE Trans. Aerospace Electron. Systems* 48, 4 (2012), 3058–3072.

[11] Sinan Gezici, Zhi Tian, G.B. Giannakis, Hisashi Kobayashi, and Zafer Sahinoglu. 2005. Localization via Ultra-Wideband Radios: A Look at Positioning Aspects for Future Sensor Networks. *IEEE Signal Processing Magazine* 22 (2005), 70–84.

[12] Wei Gong and Jiangchuan Liu. 2018. SiFi: Pushing the Limit of Time-Based WiFi Localization Using a Single Commodity Access Point. *Proc. ACM Interact. Mob. Wearable Ubiquitous Technol.* 2, 1, Article 10 (March 2018), 21 pages.

[13] Yu Gu, Jinhai Zhan, Yusheng Ji, Jie Li, Fuji Ren, and Shangbin Gao. 2017. MoSense: An RF-Based Motion Detection System via Off-the-Shelf WiFi Devices. *IEEE Internet of Things Journal* 4, 6 (Dec 2017), 2326–2341.

[14] Daniel Halperin, Wenjun Hu, Anmol Sheth, and David Wetherall. 2011. Tool Release: Gathering 802.11N Traces with Channel State Information. *SIGCOMM Comput. Commun. Rev.* 41, 1 (Jan. 2011), 53–53.

[15] Wang Hao, Zhang Daqing, Wang Yasha, Junyi Ma, Yuxiang Wang, and Shengjie Li. 2017. RT-Fall: A Real-Time and Contactless Fall Detection System with Commodity WiFi Devices. *IEEE Transactions on Mobile Computing* 16, 02 (feb 2017), 511–526.
[16] Derek Hao Hu, Sinno Jialin Pan, Vincent Wenchen Zheng, Nathan Nan Liu, and Qiang Yang. 2008. Real World Activity Recognition with Multiple Goals. In *Proceedings of the 10th International Conference on Ubiquitous Computing* (Seoul, Korea) *(UbiComp '08)*. ACM, New York, NY, USA, 30–39.
[17] Pan Hu, Liqun Li, Chunyi Peng, Guobin Shen, and Feng Zhao. 2013. Pharos: Enable Physical Analytics Through Visible Light Based Indoor Localization. In *Proceedings of the Twelfth ACM Workshop on Hot Topics in Networks* (College Park, Maryland) *(HotNets-XII)*. ACM, New York, NY, USA, Article 5, 7 pages.
[18] Harry. H. Keller. 1937. Building Structure. U.S. Patent No. 2076728A, Filed April 13., 1937, Issued.
[19] Simon Klakegg, Jorge Goncalves, Chu Luo, Aku Visuri, Alexey Popov, Niels van Berkel, Zhanna Sarsenbayeva, Vassilis Kostakos, Simo Hosio, Scott Savage, Alexander Bykov, Igor Meglinski, and Denzil Ferreira. 2018. Assisted Medication Management in Elderly Care Using Miniaturised Near-Infrared Spectroscopy. *Proc. ACM Interact. Mob. Wearable Ubiquitous Technol.* 2, 2, Article 69 (July 2018), 24 pages.
[20] Ahmed E. Kosba, Ahmed Saeed, and Moustafa Youssef. 2012. RASID: A robust WLAN device-free passive motion detection system. In *2012 IEEE International Conference on Pervasive Computing and Communications*. 180–189.
[21] Manikanta Kotaru, Kiran Joshi, Dinesh Bharadia, and Sachin Katti. 2015. SpotFi: Decimeter Level Localization Using WiFi. In *Proceedings of the 2015 ACM Conference on Special Interest Group on Data Communication* (London, United Kingdom) *(SIGCOMM '15)*. ACM, New York, NY, USA, 269–282.
[22] Ye-Sheng Kuo, Pat Pannuto, Ko-Jen Hsiao, and Prabal Dutta. 2014. Luxapose: Indoor Positioning with Mobile Phones and Visible Light. In *Proceedings of the 20th Annual International Conference on Mobile Computing and Networking* (Maui, Hawaii, USA) *(MobiCom '14)*. ACM, New York, NY, USA, 447–458.
[23] Hong Li, Wei Yang, Jianxin Wang, Yang Xu, and Liusheng Huang. 2016. WiFinger: Talk to Your Smart Devices with Finger-grained Gesture. In *Proceedings of the 2016 ACM International Joint Conference on Pervasive and Ubiquitous Computing* (Heidelberg, Germany) *(UbiComp '16)*. ACM, New York, NY, USA, 250–261.
[24] Shengjie Li, Xiang Li, Kai Niu, Hao Wang, Yue Zhang, and Daqing Zhang. 2017. AR-Alarm: An Adaptive and Robust Intrusion Detection System Leveraging CSI from Commodity Wi-Fi. In *Enhanced Quality of Life and Smart Living*, Mounir Mokhtari, Bessam Abdulrazak, and Hamdi Aloulou (Eds.). Springer International Publishing, Cham, 211–223.
[25] Xiang Li, Shengjie Li, Daqing Zhang, Jie Xiong, Yasha Wang, and Hong Mei. 2016. Dynamic-MUSIC: Accurate Device-free Indoor Localization. In *Proceedings of the 2016 ACM International Joint Conference on Pervasive and Ubiquitous Computing* (Heidelberg, Germany) *(UbiComp '16)*. ACM, New York, NY, USA, 196–207.
[26] Xiang Li, Daqing Zhang, Qin Lv, Jie Xiong, Shengjie Li, Yue Zhang, and Hong Mei. 2017. IndoTrack: Device-Free Indoor Human Tracking with Commodity Wi-Fi. *Proc. ACM Interact. Mob. Wearable Ubiquitous Technol.* 1, 3, Article 72 (Sept. 2017), 22 pages.
[27] Xiang Li, Daqing Zhang, Jie Xiong, Yue Zhang, Shengjie Li, Yasha Wang, and Hong Mei. 2018. Training-Free Human Vitality Monitoring Using Commodity Wi-Fi Devices. *Proc. ACM Interact. Mob. Wearable Ubiquitous Technol.* 2, 3, Article 121 (Sept. 2018), 25 pages.
[28] Jian Liu, Yan Wang, Yingying Chen, Jie Yang, Xu Chen, and Jerry Cheng. 2015. Tracking Vital Signs During Sleep Leveraging Off-the-shelf WiFi. In *Proceedings of the 16th ACM International Symposium on Mobile Ad Hoc Networking and Computing* (Hangzhou, China) *(MobiHoc '15)*. ACM, New York, NY, USA, 267–276.
[29] Yunhao Liu, Yiyang Zhao, Lei Chen, Jian Pei, and Jinsong Han. 2012. Mining Frequent Trajectory Patterns for Activity Monitoring Using Radio Frequency Tag Arrays. *IEEE Trans. Parallel Distrib. Syst.* 23, 11 (Nov. 2012), 2138–2149.
[30] Beth Logan, Jennifer Healey, Matthai Philipose, Emmanuel Munguia Tapia, and Stephen Intille. 2007. A Long-Term Evaluation of Sensing Modalities for Activity Recognition. In *UbiComp 2007: Ubiquitous Computing*, John Krumm, Gregory D. Abowd, Aruna Seneviratne, and Thomas Strang (Eds.). Springer Berlin Heidelberg, Berlin, Heidelberg, 483–500.
[31] Fred. A. Manske. 1935. Wall Construction. U.S. Patent No. 2000243A, Filed May 7., 1935, Issued.
[32] Wilfried Philips Hamid Aghajan Mohamed Eldib, Francis Deboeverie. 2016. Behavior analysis for elderly care using a network of low-resolution visual sensors. *Journal of Electronic Imaging* 25, 4 (2016), 1 – 17 – 17.
[33] Kai Niu, Fusang Zhang, Jie Xiong, Xiang Li, Enze Yi, and Daqing Zhang. 2018. Boosting Fine-grained Activity Sensing by Embracing Wireless Multipath Effects. In *Proceedings of the 14th International Conference on Emerging Networking EXperiments and Technologies* (Heraklion, Greece) *(CoNEXT '18)*. ACM, New York, NY, USA, 139–151.
[34] Katsunori Ohnishi, Atsushi Kanehira, Asako Kanezaki, and Tatsuya Harada. 2016. Recognizing Activities of Daily Living With a Wrist-Mounted Camera. In *The IEEE Conference on Computer Vision and Pattern Recognition (CVPR)*.
[35] Kun Qian, Chenshu Wu, Zheng Yang, Yunhao Liu, and Kyle Jamieson. 2017. Widar: Decimeter-Level Passive Tracking via Velocity Monitoring with Commodity Wi-Fi. In *Proceedings of the 18th ACM International Symposium on Mobile Ad Hoc Networking and Computing* (Chennai, India) *(Mobihoc '17)*. ACM, New York, NY, USA, Article 6, 10 pages.
[36] Kun Qian, Chenshu Wu, Zheng Yang, Yunhao Liu, and Zimu Zhou. 2014. PADS: Passive detection of moving targets with dynamic speed using PHY layer information. In *2014 20th IEEE International Conference on Parallel and Distributed Systems (ICPADS)*. 1–8.

[37] Daniele Riboni, Timo Sztyler, Gabriele Civitarese, and Heiner Stuckenschmidt. 2016. Unsupervised Recognition of Interleaved Activities of Daily Living Through Ontological and Probabilistic Reasoning. In *Proceedings of the 2016 ACM International Joint Conference on Pervasive and Ubiquitous Computing* (Heidelberg, Germany) *(UbiComp '16)*. ACM, New York, NY, USA, 1–12.
[38] Ahmed Saeed, Ahmed E. Kosba, and Moustafa Youssef. 2014. Ichnaea: A Low-Overhead Robust WLAN Device-Free Passive Localization System. *IEEE Journal of Selected Topics in Signal Processing* 8, 1 (Feb 2014), 5–15.
[39] Moustafa Seifeldin, Ahmed Saeed, Ahmed E. Kosba, Amr El-Keyi, and Moustafa Youssef. 2013. Nuzzer: A Large-Scale Device-Free Passive Localization System for Wireless Environments. *IEEE Transactions on Mobile Computing* 12, 7 (July 2013), 1321–1334.
[40] Li Shengjie, Li Xiang, Lv Qin, Tian Guiyu, and Zhang Daqing. 2018. WiFit: Ubiquitous Bodyweight Exercise Monitoring with Commodity Wi-Fi Devices. In *2018 IEEE SmartWorld, Ubiquitous Intelligence Computing(UIC)*. 530–537.
[41] Warren L Stutzman. 2018. *Polarization in electromagnetic systems*. Artech house.
[42] Ju Wang, Hongbo Jiang, Jie Xiong, Kyle Jamieson, Xiaojiang Chen, Dingyi Fang, and Binbin Xie. 2016. LiFS: Low Human-effort, Device-free Localization with Fine-grained Subcarrier Information. In *Proceedings of the 22Nd Annual International Conference on Mobile Computing and Networking* (New York City, New York) *(MobiCom '16)*. ACM, New York, NY, USA, 243–256.
[43] Wei Wang, Alex X. Liu, Muhammad Shahzad, Kang Ling, and Sanglu Lu. 2015. Understanding and Modeling of WiFi Signal Based Human Activity Recognition. In *Proceedings of the 21st Annual International Conference on Mobile Computing and Networking* (Paris, France) *(MobiCom '15)*. ACM, New York, NY, USA, 65–76.
[44] Wei Wang, Alex X. Liu, and Ke Sun. 2016. Device-free Gesture Tracking Using Acoustic Signals. In *Proceedings of the 22Nd Annual International Conference on Mobile Computing and Networking* (New York City, New York) *(MobiCom '16)*. ACM, New York, NY, USA, 82–94.
[45] Yan Wang, Jian Liu, Yingying Chen, Marco Gruteser, Jie Yang, and Hongbo Liu. 2014. E-eyes: Device-free Location-oriented Activity Identification Using Fine-grained WiFi Signatures. In *Proceedings of the 20th Annual International Conference on Mobile Computing and Networking* (Maui, Hawaii, USA) *(MobiCom '14)*. ACM, New York, NY, USA, 617–628.
[46] Yanwen Wang and Yuanqing Zheng. 2018. Modeling RFID Signal Reflection for Contact-free Activity Recognition. *Proc. ACM Interact. Mob. Wearable Ubiquitous Technol.* 2, 4, Article 193 (Dec. 2018), 22 pages.
[47] Wi-Fi Alliance 2017. . Retrieved Februray 21, 2019 from https://www.wi-fi.org/news-events/newsroom/wi-fi-in-2019
[48] Planet3 Wireless. 2005. *CWNA Certified Wireless Network Administrator Official Study Guide (Exam PW0-100)*. McGraw-Hill/Osborne.
[49] Oliver Woodman and Robert Harle. 2009. RF-Based Initialisation for Inertial Pedestrian Tracking. In *Pervasive Computing*. Springer Berlin Heidelberg, 238–255.
[50] Chenshu Wu, Zheng Yang, Zimu Zhou, Xuefeng Liu, Yunhao Liu, and Jiannong Cao. 2015. Non-Invasive Detection of Moving and Stationary Human With WiFi. *IEEE Journal on Selected Areas in Communications* 33, 11 (Nov 2015), 2329–2342.
[51] Chenshu Wu, Yang Zheng, Zimu Zhou, Kun Qian, Yunhao Liu, and Mingyan Liu. 2015. PhaseU: Real-time LOS identification with WiFi. In *Computer Communications*.
[52] C. Xiao, Y. R. Zheng, and N. C. Beaulieu. 2006. Novel Sum-of-Sinusoids Simulation Models for Rayleigh and Rician Fading Channels. *IEEE Transactions on Wireless Communications* 5, 12 (December 2006), 3667–3679.
[53] Jiang Xiao, Kaishun Wu, Youwen Yi, Lu Wang, and Lionel M. Ni. 2012. FIMD: Fine-grained Device-free Motion Detection. In *2012 IEEE 18th International Conference on Parallel and Distributed Systems*. 229–235.
[54] Jiang Xiao, Kaishun Wu, Youwen Yi, Lu Wang, and Lionel M. Ni. 2013. Pilot: Passive Device-Free Indoor Localization Using Channel State Information. In *2013 IEEE 33rd International Conference on Distributed Computing Systems*. 236–245.
[55] Wei Xu, ZhiWen Yu, Zhu Wang, Bin Guo, and Qi Han. 2019. AcousticID: Gait-based Human Identification Using Acoustic Signal. *Proc. ACM Interact. Mob. Wearable Ubiquitous Technol.* 3, 3, Article 115 (Sept. 2019), 25 pages.
[56] Moustafa Youssef, Matthew Mah, and Ashok Agrawala. 2007. Challenges: Device-free Passive Localization for Wireless Environments. In *Proceedings of the 13th Annual ACM International Conference on Mobile Computing and Networking* (Montréal, Québec, Canada) *(MobiCom '07)*. ACM, New York, NY, USA, 222–229.
[57] Zhaoyuan Yu, Linwang Yuan, Wen Luo, Linyao Feng, and Guonian Lv. 2016. Spatio-Temporal Constrained Human Trajectory Generation from the PIR Motion Detector Sensor Network Data: A Geometric Algebra Approach. *Sensors* 16, 1 (2016).
[58] Youwei Zeng, Dan Wu, Jie Xiong, Enze Yi, Ruiyang Gao, and Daqing Zhang. 2019. FarSense: Pushing the Range Limit of WiFi-Based Respiration Sensing with CSI Ratio of Two Antennas. *Proc. ACM Interact. Mob. Wearable Ubiquitous Technol.* 3, 3, Article 121 (Sept. 2019), 26 pages.
[59] Feng Zhang, Chenshu Wu, Beibei Wang, Hung-Quoc Lai, Yi Han, and K. J. Ray Liu. 2019. WiDetect: Robust Motion Detection with a Statistical Electromagnetic Model. *Proc. ACM Interact. Mob. Wearable Ubiquitous Technol.* 3, 3, Article 122 (Sept. 2019), 24 pages.
[60] Fusang Zhang, Daqing Zhang, Jie Xiong, Hao Wang, Kai Niu, Beihong Jin, and Yuxiang Wang. 2018. From Fresnel Diffraction Model to Fine-Grained Human Respiration Sensing with Commodity Wi-Fi Devices. *Proc. ACM Interact. Mob. Wearable Ubiquitous Technol.* 2, 1, Article 53 (March 2018), 23 pages.
[61] Zimu Zhou, Yang Zheng, Chenshu Wu, Sun Wei, and Yunhao Liu. 2014. LiFi: Line-Of-Sight identification with WiFi. In *Proceedings of the 33rd IEEE International Conference on Computer Communications (INFOCOM)*.

# A APPENDIX

## A.1 DCM-CSI vs. Baseline Features for Discriminating between Direct and Indirect Signals (Metal Plate Movement)

When comparing DCM-CSI against different motion detection feature, we also conducted the experiments with metal plate movement. The experimental setup and procedure are the same as the human movement experiments, except that the metal plate vibrates in-place while the human target self-rotates. Figure 26 shows the comparison in three groups of experiments for different features. Similar to human movement, only DCM-CSI is able to discriminate between direct and indirect signals. Apart from these high-level features, Figure 27 also shows the

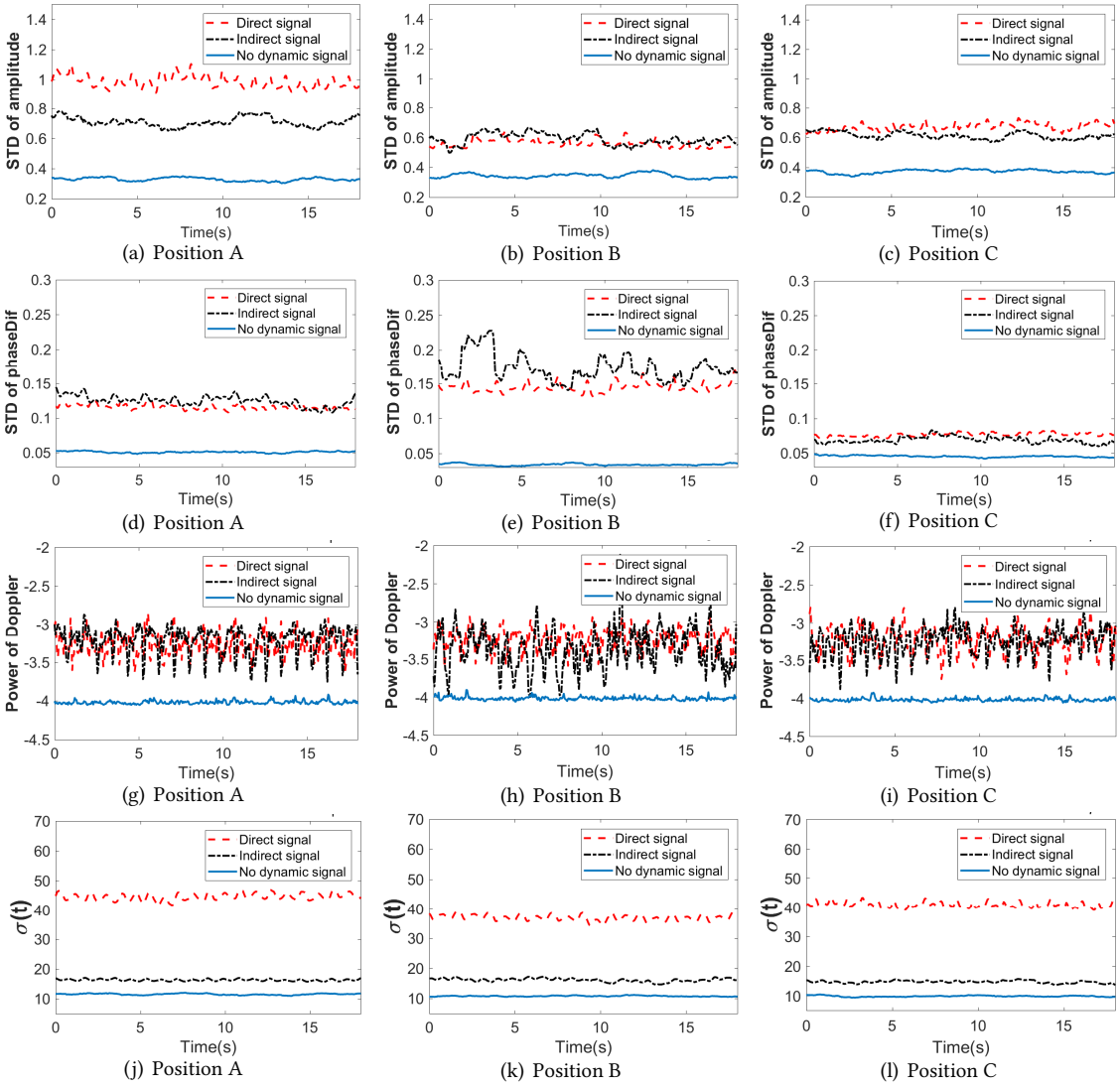


Fig. 26. Performance comparison for metal plate movement in different groups of experiments using different features: (a)-(c) Standard deviation (STD) of amplitude; (d)-(f) STD of phase difference; (g)-(i) Power of Doppler shift; and (j)-(l) DCM-CSI.

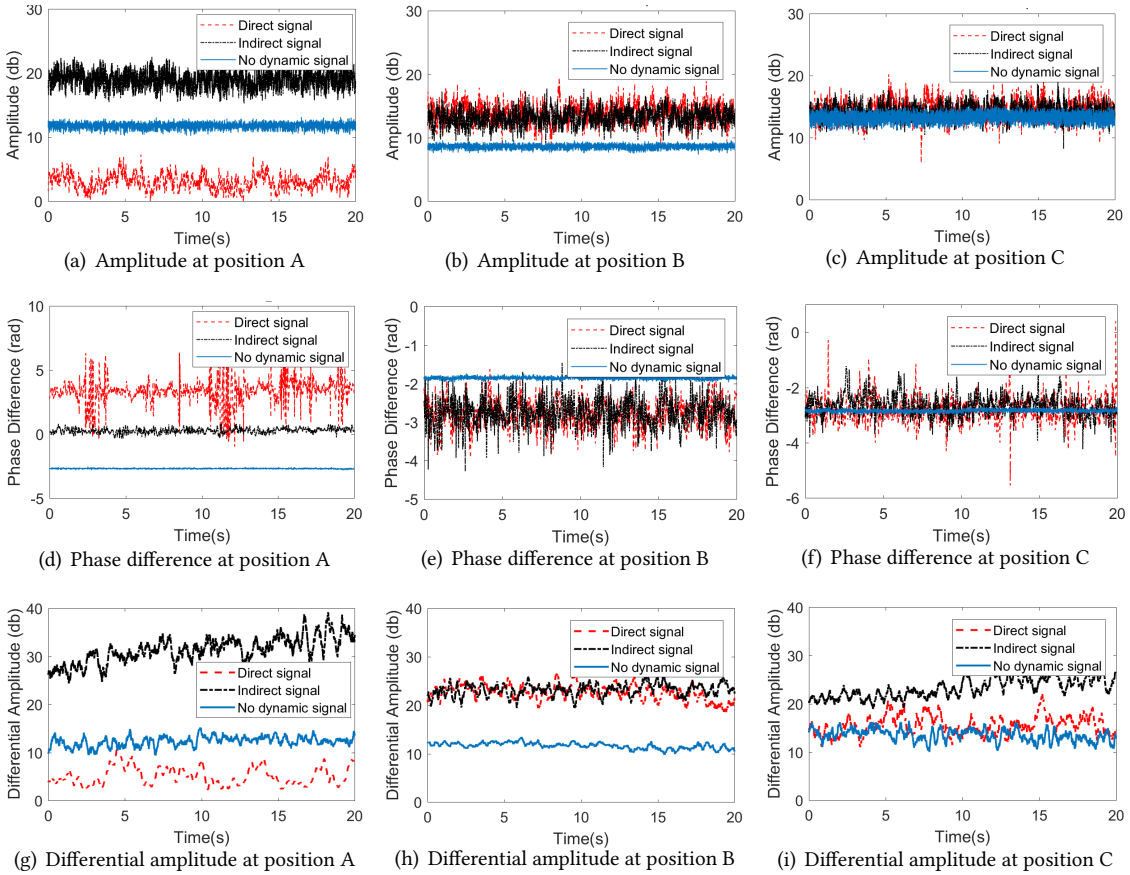


(a) Amplitude at position A (b) Amplitude at position B (c) Amplitude at position C

(d) Phase difference at position A (e) Phase difference at position B (f) Phase difference at position C

(g) Differential amplitude at position A (h) Differential amplitude at position B (i) Differential amplitude at position C

Fig. 27. Visualization of amplitude and phase difference corresponding to the comparison of human movement in Figure 6 of the Section 3.2.

raw CSI amplitude and phase difference corresponding to the comparison of human movement in Figure 6 of the Section 3.2. Additionally, we also calculate the mean amplitude of the differential of the raw complex signals (i.e., $1/T * \sum_{i=0}^{T-1} |S_t - S_{t-1}|$) as shown in Figure 27. As we can see, unlike DCM-CSI, all of these feature are difficult to differentiate the direct and indirect signals.

## A.2 Discriminating between Direct and Indirect Signals with Different Walls (Metal Plate Movement)

When studying the generality of DCM-CSI against different walls, we also conducted the experiments with metal plate. Figure 28 shows the obtained DCM-CSI's results for each wall. We can see that the gap between direct and indirect signals is obvious for all walls.

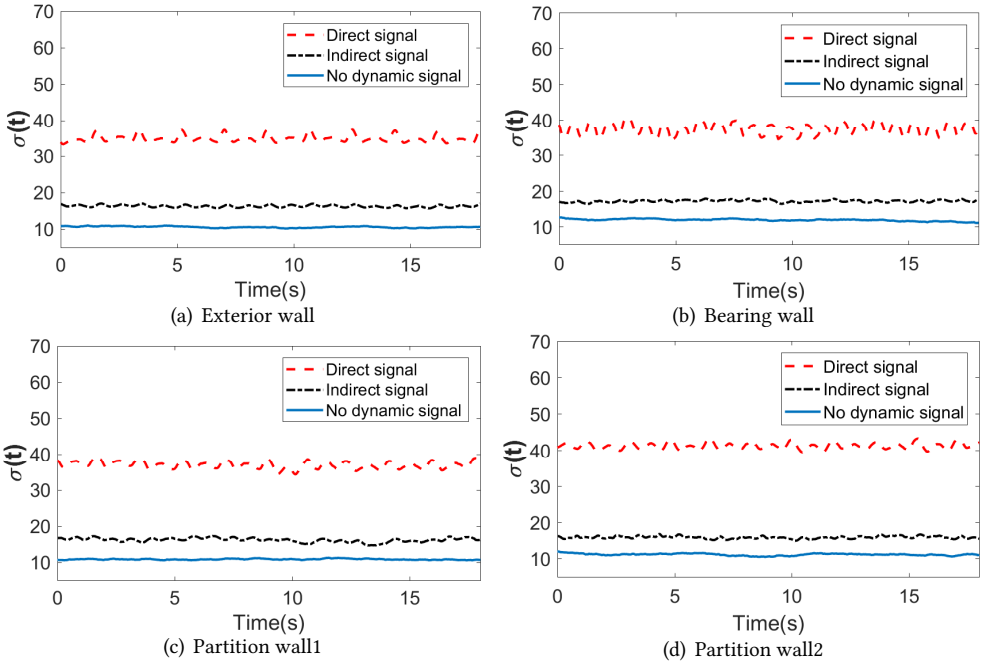


(a) Exterior wall (b) Bearing wall

(c) Partition wall1 (d) Partition wall2

Fig. 28. Using DCM-CSI for direct/indirect signal discrimination for metal plate movement against different walls.